

Old Dominion University

ODU Digital Commons

Electrical & Computer Engineering Theses & Dissertations

Electrical & Computer Engineering

Fall 1990

Optical and High Electric Field Effects in Bulk Gallium Arsenide Switches

Randy Roush
Old Dominion University

Follow this and additional works at: https://digitalcommons.odu.edu/ece_etds



Part of the [Electronic Devices and Semiconductor Manufacturing Commons](#), and the [Semiconductor and Optical Materials Commons](#)

Recommended Citation

Roush, Randy. "Optical and High Electric Field Effects in Bulk Gallium Arsenide Switches" (1990). Master of Science (MS), Thesis, Electrical & Computer Engineering, Old Dominion University, DOI: 10.25777/y9a3-ac47
https://digitalcommons.odu.edu/ece_etds/500

This Thesis is brought to you for free and open access by the Electrical & Computer Engineering at ODU Digital Commons. It has been accepted for inclusion in Electrical & Computer Engineering Theses & Dissertations by an authorized administrator of ODU Digital Commons. For more information, please contact digitalcommons@odu.edu.

OPTICAL AND HIGH ELECTRIC FIELD EFFECTS IN BULK GALLIUM
ARSENIDE SWITCHES

by

Randy Roush
B.S. in Electrical Engineering, May 1989
Old Dominion University, Norfolk, Virginia

A Thesis Submitted to the Faculty of
Old Dominion University in Partial Fulfillment of the
Requirements for the Degree of

MASTER OF SCIENCE

ELECTRICAL ENGINEERING

with an emphasis on Physical Science

OLD DOMINION UNIVERSITY
December, 1990

Approved by:

Dr. Karl Schoenbach (Director)

R.Joshi

Vishnu K. Lakdawala

ABSTRACT

OPTICAL AND HIGH ELECTRIC FIELD EFFECTS IN BULK GALLIUM ARSENIDE SWITCHES

Randy Roush
Old Dominion University
Director: Dr. Karl Schoenbach

During the past few years, bulk, photoconductive switching has become recognized as a viable topic for future research on moderate and high power switches. The two-pulse, or BOSS, concept relies on an excitation laser pulse, and a separate de-excitation pulse in conjunction with silicon doped, copper compensated, GaAs to create a variable temporal electrical pulse width. The research contained in this document provides information concerning the feasibility of the BOSS concept, as the switch is scaled to larger sizes, and higher voltage and current. The major concern will be the high voltage and current effects. The absorption length for 1064 nm laser light in GaAs has been determined in order to design contacts that allows for maximum voltage hold-off. At higher voltages, an effect known as lock-on has been observed and is extensively studied here. Specifically, the temporal development of the dark lock-on current, and infrared quenching of lock-on currents will be addressed. Results of experimental and theoretical studies on thermal effects and steady-state dark current-voltage curves are presented. Experiments demonstrating infrared quenching of lock-on currents have been conducted.

ACKNOWLEDGEMENTS

I thank Dr. Karl Schoenbach for his guidance in this research and giving me the opportunity to work with his group. I also thank Dr. Lakdawala and Dr. Joshi for being part of my committee. I thank Dr. Mike Mazzola for giving his time to teach an ex-baseball player to become an engineer. I also thank Dr. Ralf Peter Brinkmann for the extensive amount of time he has spent discussing different issues concerning this research. Thanks to Steve Dean, Benny Stokes, Sung Kim, and Gordhan Barevadia for making the laser lab a productive and enjoyable place to work. A special thanks goes to my parents for giving me their continuous support and encouragement. As any good researcher should, I must thank my new wife Chari' for her patience, inspiration, and for helping me find the library. Finally, I thank the Cincinnati Reds for winning the Series in four games, because if it had lasted seven this thesis might not have been finished on time.

The research contained in this document was supported by SDIO/IST and managed by ONR.

TABLE OF CONTENTS

	<i>Page</i>
ACKNOWLEDGEMENTS	ii
TABLE OF CONTENTS	iii
LIST OF TABLES	v
LIST OF FIGURES	vi
LIST OF SYMBOLS	ix
 <i>Chapters</i>	
1. INTRODUCTION	1
1.1 Background	1
1.2 BOSS Concept	3
1.3 Topics to be Covered	7
2. ABSORPTION OF INFRARED RADIATION IN GaAs:Si:Cu ...	12
2.1 Introduction	12
2.2 Theory	14
2.3 Experiment and Results	19
2.4 Summary	33
3. DARK CURRENT	35
3.1 Introduction	35
3.2 Thermal Effects	36
3.3 Double Injection	47
3.4 Experiments and Results	57
3.5 Discussion	69

TABLE OF CONTENTS - concluded

4. INFRARED QUENCHING OF LOCK-ON CURRENTS	71
4.1 Theory	71
4.2 Experiments and Results	74
4.3 Discussion	79
5. CONCLUSIONS	84
5.1 Discussion of Results	84
5.2 Future Work	90
5.3 Final Remarks	91
LIST OF REFERENCES	92
APPENDIX A	97

LIST OF TABLES

<i>Table</i>		<i>Page</i>
2-1	Characteristics of samples used in the absorption measurements	20
3-1	Physical properties of the samples used in the experiments . . .	42
3-2	Material parameters used in the simulations	51

LIST OF FIGURES

<i>Figure</i>	<i>Page</i>
1-2-1 Energy band diagram for silicon doped, copper compensated gallium arsenide (GaAs:Si:Cu)	4
1-2-2 The BOSS switching cycle	6
1-2-3 The compensation curve for copper in silicon doped gallium arsenide [12].	8
1-2-4 The results of a rate equation model based on the BOSS concept [12]	9
1-2-5 The experimental results of the BOSS concept. Note the similarities between the experimental and theoretical results [11]	10
2-1-1 Planar (top) and Over-Under (bottom) contact geometries	13
2-2-1 Traversal of light through the crystal with internal reflections	17
2-3-1 A typical laser pulse from the DCR-3	21
2-3-2 The experimental set-up for the absorption measurements	23
2-3-3 Traversal of light with non-normal angle of incidence	24
2-3-4 Photodiode bias circuit	28
2-3-5 Photodiode response as a function of laser intensity	29
2-3-6 Results of the absorption measurements for GaAs:Si, GaAs:Si:Cu, and semi-insulating GaAs	31
3-2-1 Expected I-V curve (solid line) and the thermal stability curve (dashed line)	40

LIST OF FIGURES - continued

3-2-2	Current-Voltage curves for sample 1297-14-A10 in different thermal environments	44
3-2-3	The temporal decay of the current after a heat source was removed. The sample environment was air	46
3-3-1	The I-V curves for simulations #1 (top) and #2 (bottom)	52
3-3-2	The I-V curves for simulations #3 (top) and #4 (bottom)	54
3-3-3	The I-V curves for simulations #5 (top) and #6 (bottom)	55
3-3-4	The I-V curves for simulations #3 (top) and #4 (bottom) under irradiation	56
3-4-1	Sample 1297-10-A10 current waveform resulting from an applied bias voltage of 40 μ s duration	58
3-4-2	The transmission line pulser circuit used to apply 300 ns and 600 ns pulses to the samples	61
3-4-3	A series of current waveforms resulting from various applied bias voltages. The bias voltage corresponding to waveform <i>b</i> is larger than that for waveform <i>a</i>	62
3-4-4	The current waveform for the curve labeled <i>a</i> (top) in figure 3-4-3 with the corresponding applied voltage waveform (bottom)	63
3-4-5	The dark current onset time vs the applied bias voltage	64
3-4-6	The I-V curve for sample 1297-10-A5	66
3-4-7	Current just after the fast transition vs applied bias just before the fast transition (top) and the same current vs the voltage just after the fast transition (bottom).	67
3-4-8	The I-V curve for sample 1297-10-A10	68
4-1-1	Band diagram for GaAs:Si:Cu with the traps filled	72
4-2-1	Photocurrent decay with applied fields below and above the lock-on threshold (top and bottom curves respectively)	75

LIST OF FIGURES - concluded

4-2-2	The bias circuit for use in the photoconductive experiments	76
4-2-3	The I-V curve for the photocurrent data (see figure 4-2-1)	78
4-2-4	Infrared quenching of lock-on photocurrent	80
4-2-5	Infrared quenching of photocurrent below the lock-on threshold . .	81
4-3-1	A hypothetical dark current curve (solid line) plotted together with the experimental I-V data from figure 4-2-3. The imposed load lines are shown with dashed lined	82
5-2-1	The I-V curve showing negative differential conductivity with various load lines for a fixed bias voltage	88

LIST OF SYMBOLS

Symbol

α	Absorption coefficient
C	Specific heat
Cu_A	Copper A level in GaAs
Cu_B	Copper B level in GaAs
C_m	Heat capacity
d	Sample length
d_{eff}	Effective traversal length
E	Electric field strength
E_a	Energy of an arbitrary acceptor level
E_g	Bandgap energy
$EL2$	Known defect level in GaAs
ϵ	Permittivity of the material
ϵ_o	Permittivity of free space
ϵ_r	Relative permittivity
Γ	Heat loss to the environment
h	Planck's constant
i	Current
I_o	Incident light intensity

LIST OF SYMBOLS - continued

I_T	Transmitted light intensity
J	Current Density
J_n	Electron current density
J_p	Hole current density
k	Defined variable
K	Lattice thermal conductivity
L	Light intensity (Chapter 2)
l	hypotinus length for the light traversal
λ	Time constant of the instability
μ	Permeability of the material
μ_n	Electron mobility
μ_p	Hole mobility
n	electron density
N	Number of reflections
n_{air}	Index of refraction for air
N_a	Density of an arbitrary acceptor level
n_{GaAs}	Index of refraction for GaAs
n_{Glass}	Index of refraction for glass
p	Hole density
P	Power dissipated
ρ	Charge density
ρ	Crystal density

LIST OF SYMBOLS - concluded

$\delta\rho$	Change in fixed charge density in the crystal
q	Electrical charge
R	Reflection coefficient (Chapter 2)
R	Resistance (Chapters 3 - 5)
R_0	Initial Resistance
r_n	Steady state recombination rate for electrons
r_p	Steady state recombination rate for holes
SF_6	Sulfur Hexafluoride
T	Transmission coefficient
ΔT	Temperature change (from room temperature) in a crystal
T^*	Constant with units of temperature
τ	Time constant
θ_c	Critical angle for total internal reflection
θ_i	Angle of incidence
θ_r	Angle of refraction
V	Voltage
ν	Frequency of light
v_n	Drift velocity of electrons
v_p	Drift velocity of holes

CHAPTER 1

INTRODUCTION

1.1 BACKGROUND

Switches are an intricate part of any electrical system and a major concern within the pulsed power community. The ideal switch operates with no voltage drop when *on*, no leakage current when *off*, and zero rise and fall times. Thyristors such as semiconductor controlled rectifiers (SCR's) are readily available for low power applications and they serve their purpose very well. At moderate and high powers, slow recovery caused by the high forward currents, and high bias voltages make the SCR a bit less desirable. Triggering SCR stacks becomes a problem at higher powers and isolation presents still another challenge. Other switches such as vacuum and gas filled tubes are widely used for moderate power applications. These devices have a relatively high on-state resistance and their recovery characteristics make them impractical in many applications. Thyratrons, for instance, are cumbersome because of their size and the need for grid heating. High voltage switch applications generally make use of spark gaps which rely on either over-voltage or field distortion for triggering a gas breakdown between two electrodes. Spark gap design has been a major research focus for many groups over the past few decades.

Research and development in the switching field must be directed towards devices that will serve the needs of low, moderate, and high power applications. It is apparent now that the moderate and high power switching is somewhat poorly served by the switches readily available today. Also the need for fast opening switches is quickly growing. Uses in inductive energy storage systems, and applications in high resolution pulsed radar systems are candidates for the implementation of fast closing and opening switches. Efforts have been made to develop an optically controlled switch using gallium arsenide because of its superior electrical properties compared to other semiconductor materials such as silicon. Gallium arsenide is a direct bandgap semiconductor, which allows for extremely fast electrical characteristics. The mobility of electrons is in the range of $5000 \text{ cm}^2/\text{V}\cdot\text{s}$. An optically controlled switch provides superior switching times compared to other methods, and complete electrical isolation of the system. Opto-thyristors have been studied by other groups and seem to have some attractive features [1].

Studies related to the use of bulk gallium arsenide have been previously carried out [2,3]. Much of the research has involved sustained photoconductivity during illumination by a laser pulse of photon energy greater than the bandgap energy of the semiconductor. Losses due to recombination require the optical excitation source to illuminate the switch during the entire electrical pulse width. Recombination times may be on the order of picoseconds in gallium arsenide due to the presence of recombination centers in the material [4]. As one might expect, a tremendous amount of laser radiation is needed to maintain the switch closure against the recombination process. However, if the desired electrical pulse is to

resemble the laser pulse temporally, then constant illumination may have some merit. The use of expensive laser sources is still rather impractical in many cases, however relatively cheap electron beams have been used as irradiation sources for bulk gallium arsenide switches [5,6]. The generated electrical pulses in this case can also resemble the excitation pulse temporally. For very fast closing and opening applications, relatively intense, fast, laser pulses are required. The limitation for the use of GaAs as high power opening switches is an effect known as "lock-on" which will be discussed in detail in chapters 3 and 4. Appendix A briefly discusses the origins of the lock-on effect as well a few theories concerning the physics of the effect.

A concept which does not rely on the temporal shape of the laser pulse to determine the temporal shape of the electrical pulse, is called the Bulk Optically Controlled Semiconductor Switch (BOSS) [7,8,9]. The BOSS involves bulk gallium arsenide doped with silicon and compensated with diffused copper. Optical closing and opening provides extremely fast rise and fall times [10]. The advantage here is that laser energy is not required to sustain the photocurrent. Optical energy is only required to generate and quench the current.

1.2 BOSS CONCEPT

Copper forms several deep acceptor levels in silicon doped gallium arsenide including one at 0.14 eV and another at 0.44 eV from the valence band (see figure 1-2-1). These deep acceptors trap free electrons provided by the silicon donor which effectively moves the Fermi-level closer to the middle of the bandgap. The diffusion

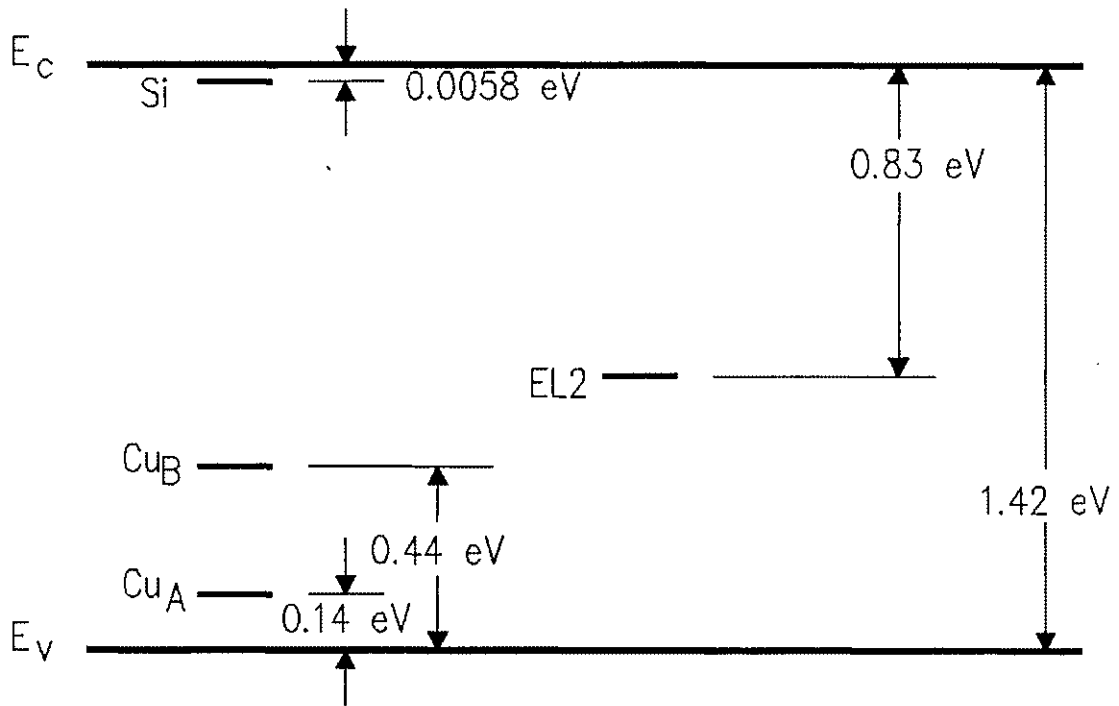


Figure 1-2-1. Energy band diagram for silicon doped, copper compensated gallium arsenide (GaAs:Si:Cu).

of copper is therefore a critical process in the development of the switch. Controlled compensation of GaAs:Si has been shown previously [11]. For switch closure, the electrons trapped at the Cu_B level may be optically excited into the conduction band using the proper laser radiation. With a bandgap energy in gallium arsenide of 1.42 eV, the energy difference between the conduction band and the copper level Cu_B is 0.98 eV. The photon energy required to move an electron to the conduction band must then be greater than 0.98 eV. The switch concept is summarized in figure 1-2-2. An incident laser pulse containing sufficient energy will move electrons up to the conduction band and holes down to the valence band (figure 1-2-2 (a)). The optical cross-sections and recombination kinetics in the material ensure that a significant net electron density remains in the conduction band for typical times of microseconds [7]. Two other parameters of interest are the capture cross-sections for electrons and holes. The ratio of the capture cross sections for free holes to free electrons is about 10^6 which makes the level a hole trap [7]. This allows the generated photocurrent to persist for long times compared to the optical pulse (figure 1-2-2 (b)). Complete infrared quenching of the photocurrent has been accomplished using this material [10]. Opening of the switch involves the optical ionization of holes from the copper level into the valence band giving rise to fast recombination with conduction electrons and a strong quench (figure 1-2-2 (c)). Due to the difference in optical excitation cross-sections between the electrons and holes at the copper center, a higher photon flux is required to ionize holes into the valence band.

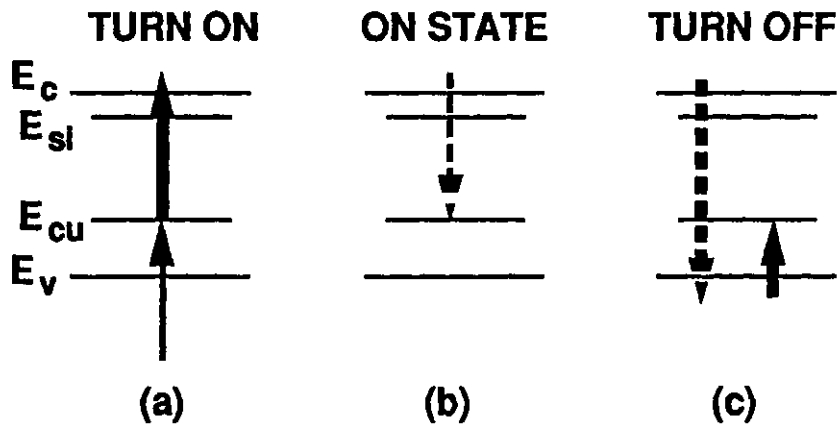


Figure 1-2-2. The BOSS switching cycle.

Switching results

Based on the level of compensation in the switch material, either a p-type or an n-type switch may be formed (figure 1-2-3) [12]. Figure 1-2-4 shows the results of a rate equation model which displays the difference in responses of the theoretical switch to a 1 eV laser pulse for the two material types [12]. The experimental results (figure 1-2-5) show a good correlation between experiment and theory. These results were obtained for electric fields of less than 100 V.

1.3 TOPICS TO BE COVERED

Now that the switch concept has been shown to work at low electric fields, the next challenge is to provide information that will lead to a practical device. Practical should mean operation at thousands of volts and thousands of amperes. At higher voltages, however, the switch operates in a state known as "lock-on" which is characterized by persistent photocurrents (see Appendix A) [13].

The laser sources needed to trigger the device must be cost efficient. Sources such as diode lasers are very attractive because of their low cost and high speed. The problem is finding a low cost laser source that delivers fast (ns) pulses with sufficient intensity. The laser radiation must also be able to penetrate the bulk of the material in order to ionize the volume between the contacts. The following chapters will be concerned with some of the issues which need to be addressed before the BOSS concept will be made practical. First, chapter 2 will cover the absorption of radiation in the switch material and its effect on the contact geometry, and the geometric scaling of the switch. Chapters 3 and 4 will address the most

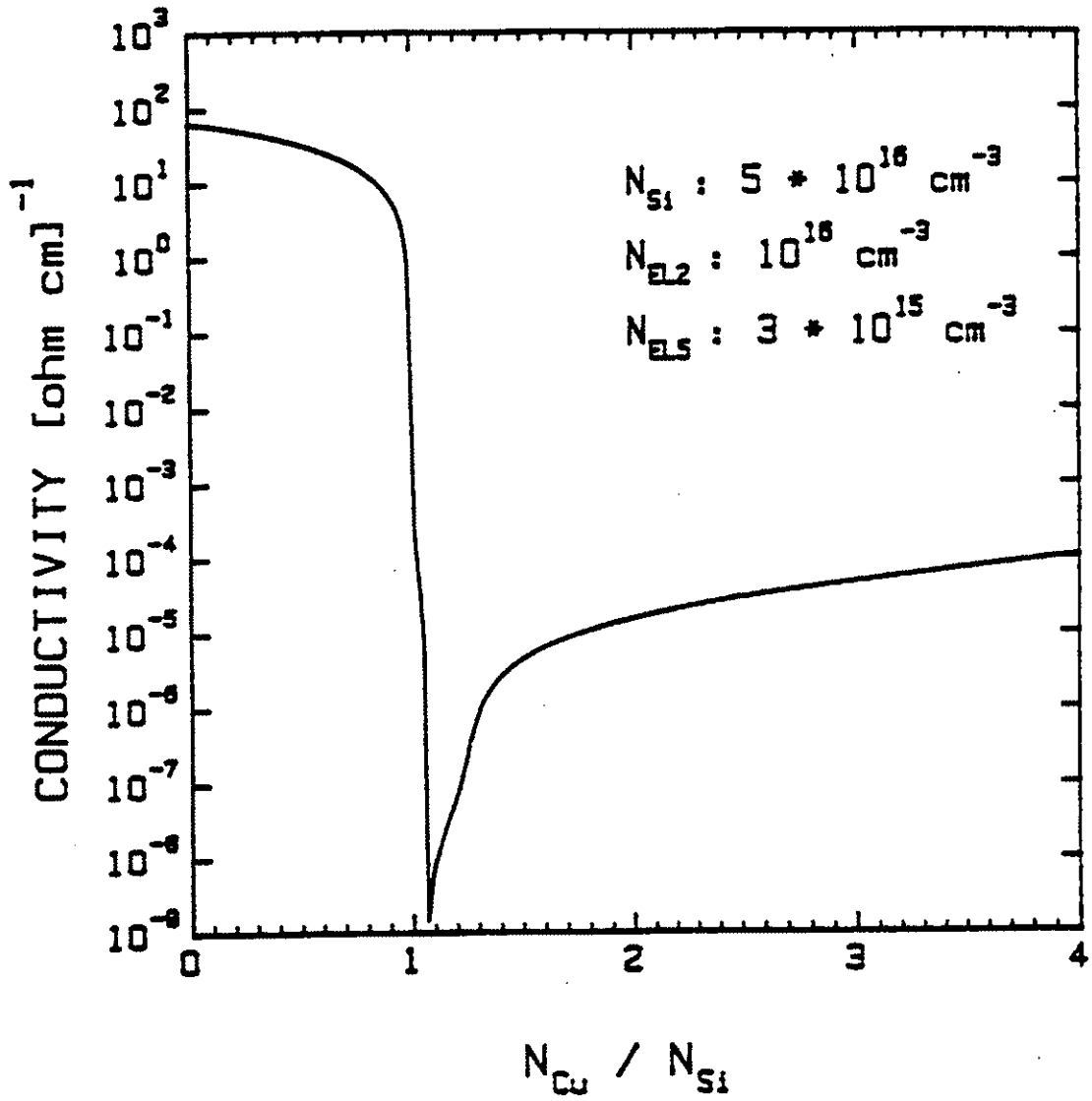


Figure 1-2-3. The compensation curve for copper in silicon doped gallium arsenide.

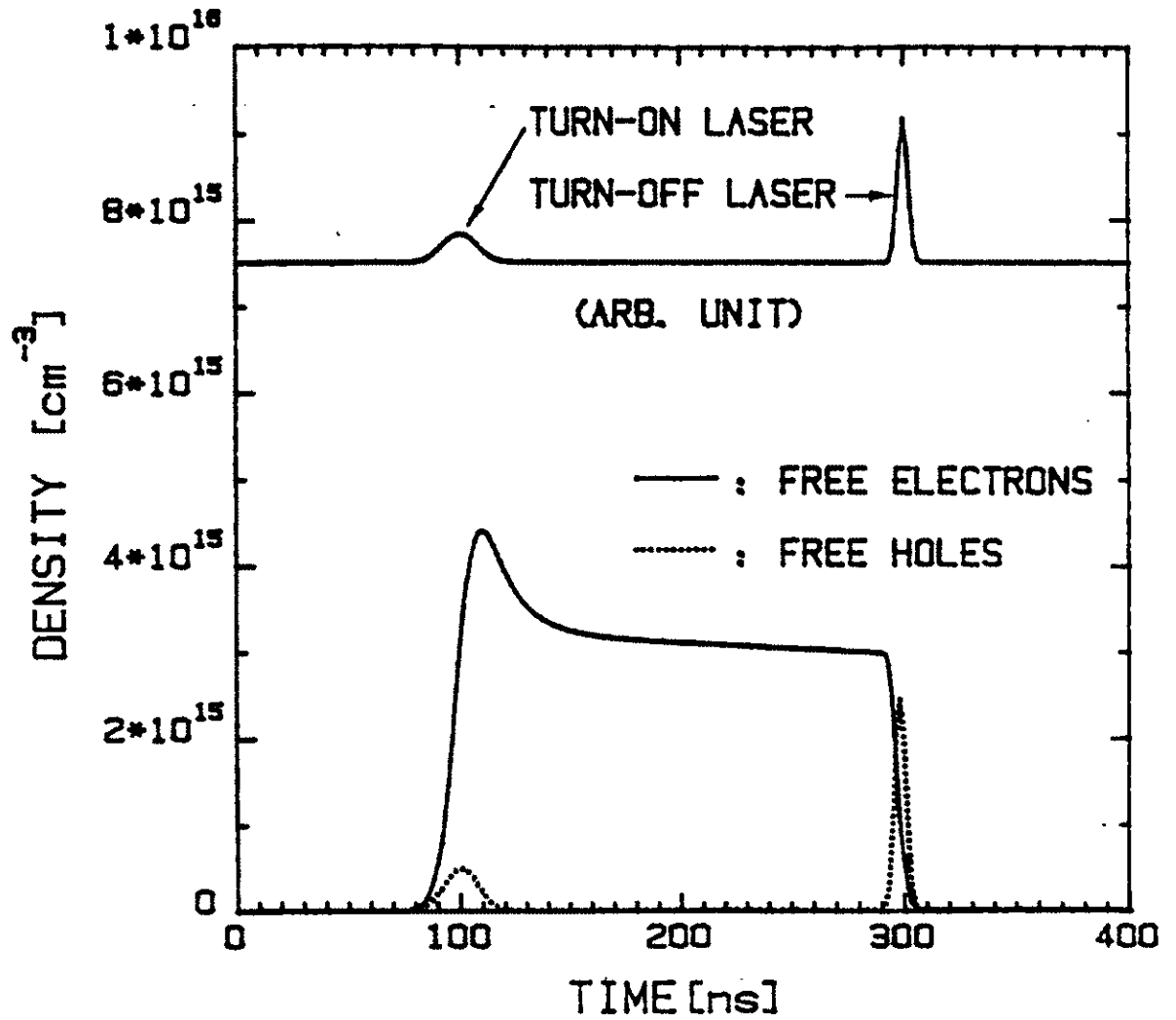


Figure 1-2-4. The results of a rate equation model based on the BOSS concept.

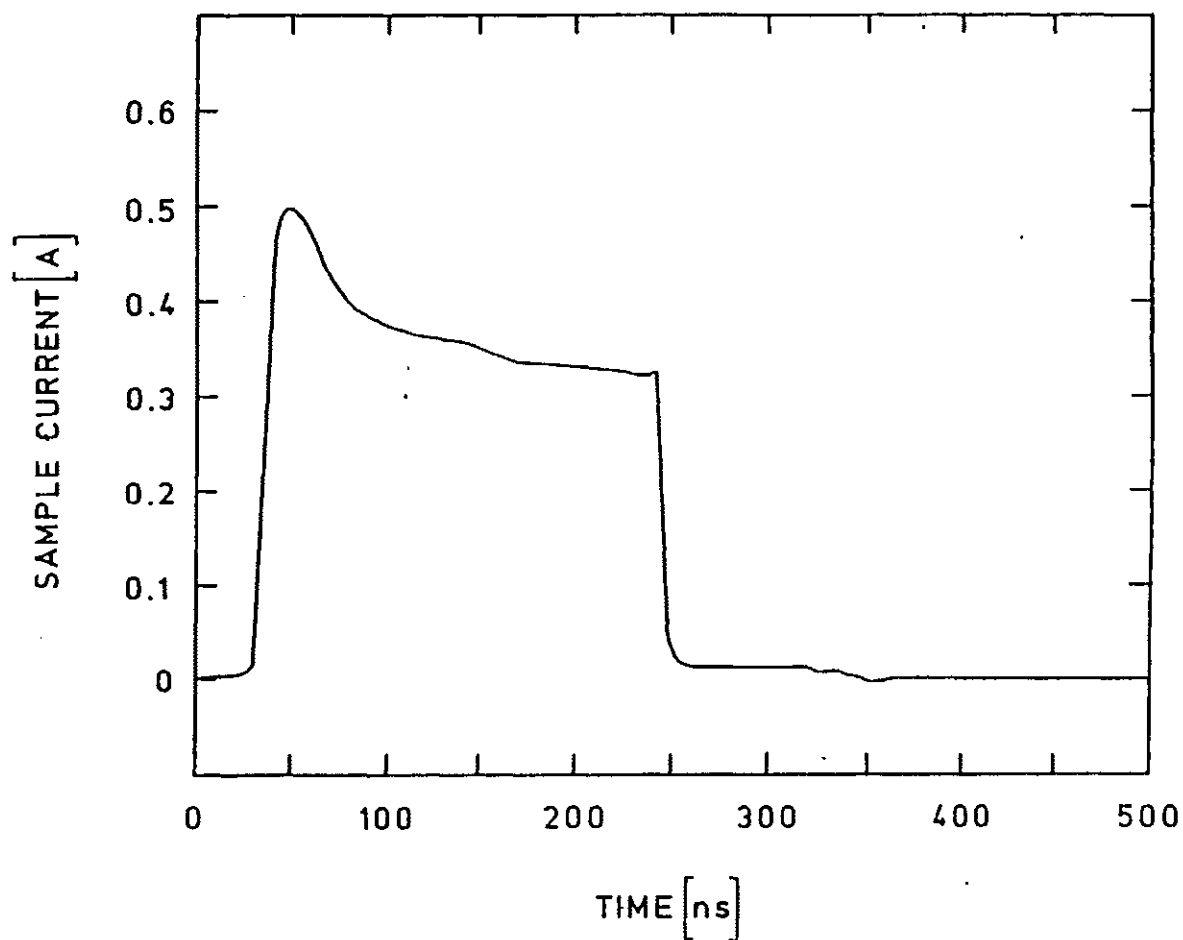


Figure 1-2-5. The experimental results of the BOSS concept. Note the similarities between the experimental and theoretical results (see figure 1-2-4).

challenging topic: the lock-on effect. First, chapter 3 presents the theory and results concerning the dark current characteristics. This chapter involves, thermal effects, DC and transient current-voltage curves, and a method for modeling the electrical characteristics of the switch with data resulting from a model developed at Old Dominion University. Chapter 4 will present experimental data concerning the quenching of lock-on currents in GaAs:Si:Cu. The quenching of photocurrents and dark currents will be discussed.

CHAPTER 2
ABSORPTION OF INFRARED RADIATION
IN GaAs:Si:Cu

2.1 INTRODUCTION

In the low power switching experiments, the choice of contact geometry involves a few simple considerations. First, the magnitude of the electric field to be held off will become important. Second, the possible contact geometries must be explored in relation to the maximum electric field to be held off. Third, the penetration depth of the incident laser pulse is a factor that requires consideration before the contact geometry can be chosen. Two geometries will be discussed here: planar and over-under (see Figs. 2-1-1(a) and 2-1-1(b)), and variations of these will be discussed.

For the planar geometry, the current will be conducted across the surface of the material which is not a problem at low voltages. Also, turning the switch on requires the incident laser pulse to ionize an area between the contacts, but does not require the light to penetrate the surface of the switch to any large degree. Surface effects, in this case, must be considered. Surface flash-over limits the use of the planar contacts to low field applications. Planar contacts may be used with care at higher voltages if the switch environment is changed. The magnitude of the field that

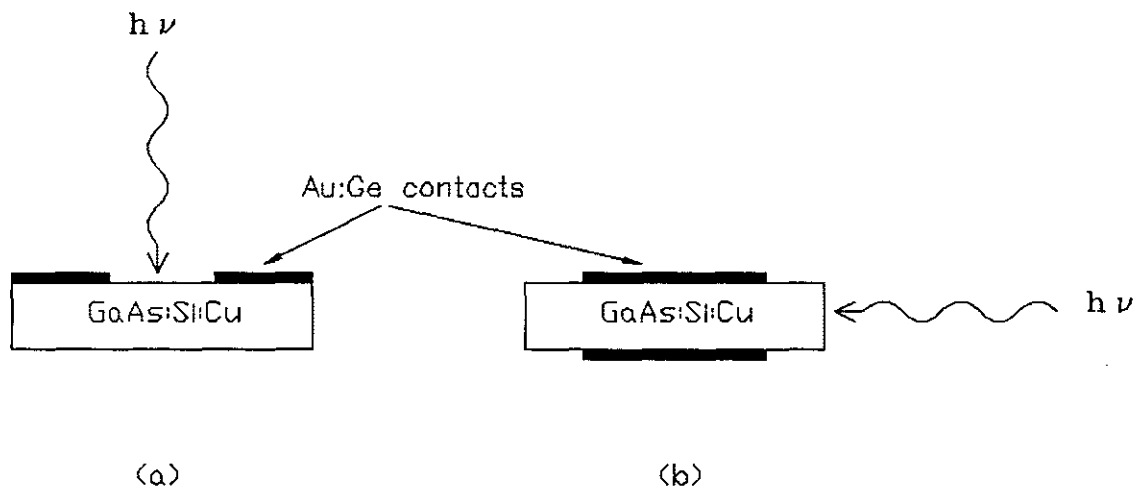


Figure 2-1-1. Planar (a) and Over-Under (b) contact geometries.

can be held off is dependent on the gap spacing, switch environment, and the quality of the contact edges. Placing the sample in an environment of SF₆ or transformer oil, for example, will allow higher fields to be applied.

The over-under contact geometry (figure 2-1-1 (b)) offers the advantages of smaller distance between the contacts and a greater distance across which surface flash-over can occur. The major concern with this type of contact geometry is the penetration depth of the incident laser pulse used for switch excitation. If the absorption of radiation is substantial, ionization of the volume between the contacts will not occur and the switch efficiency will be sacrificed. Since high electric field effects are to be examined in later chapters, the over-under contacts are chosen, and the penetration depth of infrared radiation in GaAs:Si:Cu will be considered in this chapter.

2.2 THEORY

Absorption of radiation in semiconductors allows many material parameters to be found. The most common application for absorption measurements is in absorption spectroscopy, which is a way of probing the bandgap of the semiconductor in order to find impurity and defect levels. Each energy level in the bandgap contains a certain density of bound charges (electrons or holes). Some possible transitions that an electron or hole may undergo are band-to-band (fundamental), exciton, between sub-bands, and between impurities and bands. Absorption will be referred to in terms of α which is a function of the photon energy. The absorption coefficient is defined as,

$$\alpha = \frac{1}{L} \frac{dL}{dx} \quad (2.2.1)$$

where L is the light intensity which is a function of the photon energy. Equation 2.2.1 implies that the light intensity will decrease exponentially as it passes through the sample.

Fundamental, or band-to-band, transitions are due to the ionization of an electron from the valence band to the conduction band. A very sharp increase in the absorption coefficient should be observed as the photon energy approaches the bandgap energy. In this case, there may be zero absorption for photon energies less than the bandgap energy. Such a situation, however, does not exist due to the presence of impurity and defect levels in the bandgap. In GaAs, it may be shown that the absorption close to the band edge is controlled by impurity levels in the material [14]. Therefore, the doping of impurities has a large effect on the absorption of radiation with quantum energies below the bandgap energy.

Transitions between a band and an impurity level is of great interest because it is the mechanism which allows the *BOSS* concept to work. Consider the band diagram shown in figure 1-2-1 which displays the various energy levels in GaAs:Si:Cu. If the incident photon energy is greater than the energy difference between the copper level and the conduction band, electrons may be excited into the conduction band. Transitions from the valence band to the empty sites at the impurity level must also be considered. This implies that for a given impurity concentration and an incident laser pulse of sufficient photon energy, a net flux of electrons will either enter or leave the impurity level. The photo-ionization cross sections for electrons

and holes at the impurity level will determine which process dominates. For example, in GaAs the photo-ionization cross section for electrons is about an order of magnitude less than that for holes. The $h\nu$ dependence of the absorption coefficient with the effect of an acceptor level is,

$$\alpha \propto N_a(h\nu - E_g + E_a)^{1/2} \quad (2.2.2)$$

In the following sections, the penetration depth of 1064 nm laser radiation will be measured in gallium arsenide with different doping profiles. The addition of copper atoms in the host crystal, GaAs:Si, will cause a change in the absorption depth for the incident laser radiation with a wavelength of 1064 nm. This result will provide evidence that copper controls the absorption characteristics which is the desired result for the operation of the photoconductive *BOSS* switch.

Transmission Equation

The transmission characteristics derived are based on multiple reflections in the solid as shown in figure 2-2-1. The transmission is defined as the ratio of the incident to transmitted intensities. The radiation is partially transmitted after striking the surface of the sample which leaves an intensity of $I_0(1-R)$ at point *a* in figure 2-2-1. Point *b* corresponds to the first traversal of the light into the material which must be accompanied by an exponential decay of the intensity, $I_0(1-R)e^{-\alpha d}$. Only a small fraction of these surviving photons will emerge from the sample, point *c*, and may be expressed as $I_0(1-R)^2e^{-\alpha d}$. Taking all reflections into account, the total transmission may be expressed as

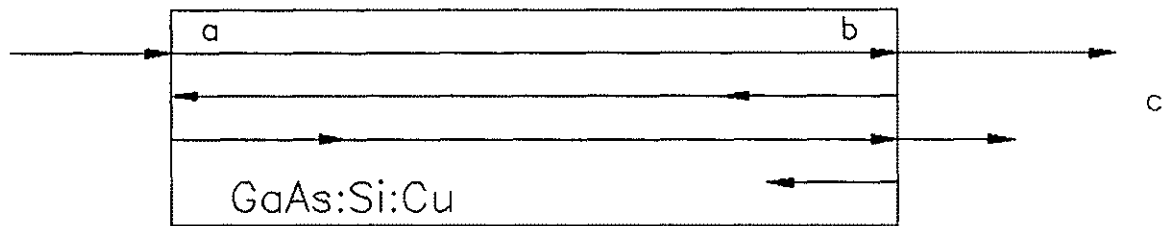


Figure 2-2-1. Traversal of light through the crystal with internal reflections.

$$T = \frac{(1-R)^2 e^{-\alpha d}}{1 - R^2 e^{-2\alpha d}} \quad (2.2.3)$$

[15]. This equation may be simplified if it is assumed that the αd term is large, in which case the equation for the transmission will become,

$$T \sim (1-R)^2 e^{-\alpha d} \quad (2.2.4)$$

The initial conditions such as surface quality, doping profile, free carrier concentration and type, sample length, and sample height are important contributors to the absorption characteristics. Surface effects involving dangling bonds from cleavage of the sample will degrade the absorption length [16]. Some studies have been performed to determine the effect of surface imperfections resulting from cleaving various semiconductors [17]. Free carrier absorption (similar to intraband absorption) also needs to be considered. Free carrier absorption involves moving an electron (for example), already in the conduction band, to a higher energy state within the conduction band. This absorption mechanism is proportional to the number of carriers per unit volume [18]. If the number of carriers per unit volume is relatively small, then the absorption due to those carriers will be minimal. In the case of copper doped, semi-insulating GaAs, the free carrier absorption will be neglected.

In any case, the losses due to absorption need to be investigated experimentally. The following sections will discuss an experiment to measure the absorption coefficient (α) of infrared radiation in GaAs of different doping profiles.

2.3 EXPERIMENT AND RESULTS

From the above equations, the measurement of the transmission, and thus the absorption coefficient, seems to be fairly simple. Application of a laser pulse of known intensity and measurement of the transmitted intensity would provide the required information, however experiments are often deceiving in their apparent simplicity. For instance, in this case, the sample thickness was 0.5 mm which provides difficulty in measurement. The samples are classified in table 2-1 by name according to thickness, and doping profile. Measurement of the transmitted intensity was accomplished with the samples listed in table 2-1 and will now be described.

The laser to be used is a commercial system manufactured by spectra physics. The system uses a DCR-3 Nd:YAG (fundamental wavelength of 1064 nm) laser head which is capable of delivering 1 Joule of energy in a pulse with a full width at half maximum (FWHM) of 10 ns. The output pulse has a mode structure of TEM_{01} which has the basic shape of a donut. A typical laser pulse from this system is shown temporally in figure 2-3-1. The energy needed for this experiment is much less than 1 J so the DCR-3 was operated at less than 100 mJ. The diameter of the output laser pulse of approximately 1 cm^2 is much greater than the area of the incident edge of the GaAs:Si:Cu sample. This presents the problem of light *leaking* around the sample and being detected as transmitted light.

A TEM_{01} pulse is a rather undesirable mode structure for this experiment because of the relative difficulty in alignment and repeatability. A more advantageous mode structure would actually be a lack of any definite mode structure, or, in other words, multi-mode. This greatly facilitates the alignment procedure. An

Table 2-1. The physical properties of the samples used in the absorption measurements *

Sample Name	Dopants	Cu Diffusion Time, Temperature [hours],[°C]	Initial Sample Length [cm]
1297-13-A1	Si	-	2
1297-13-A2	Si, Cu	15, 575	1

* These samples were taken from the same wafer, side-by-side

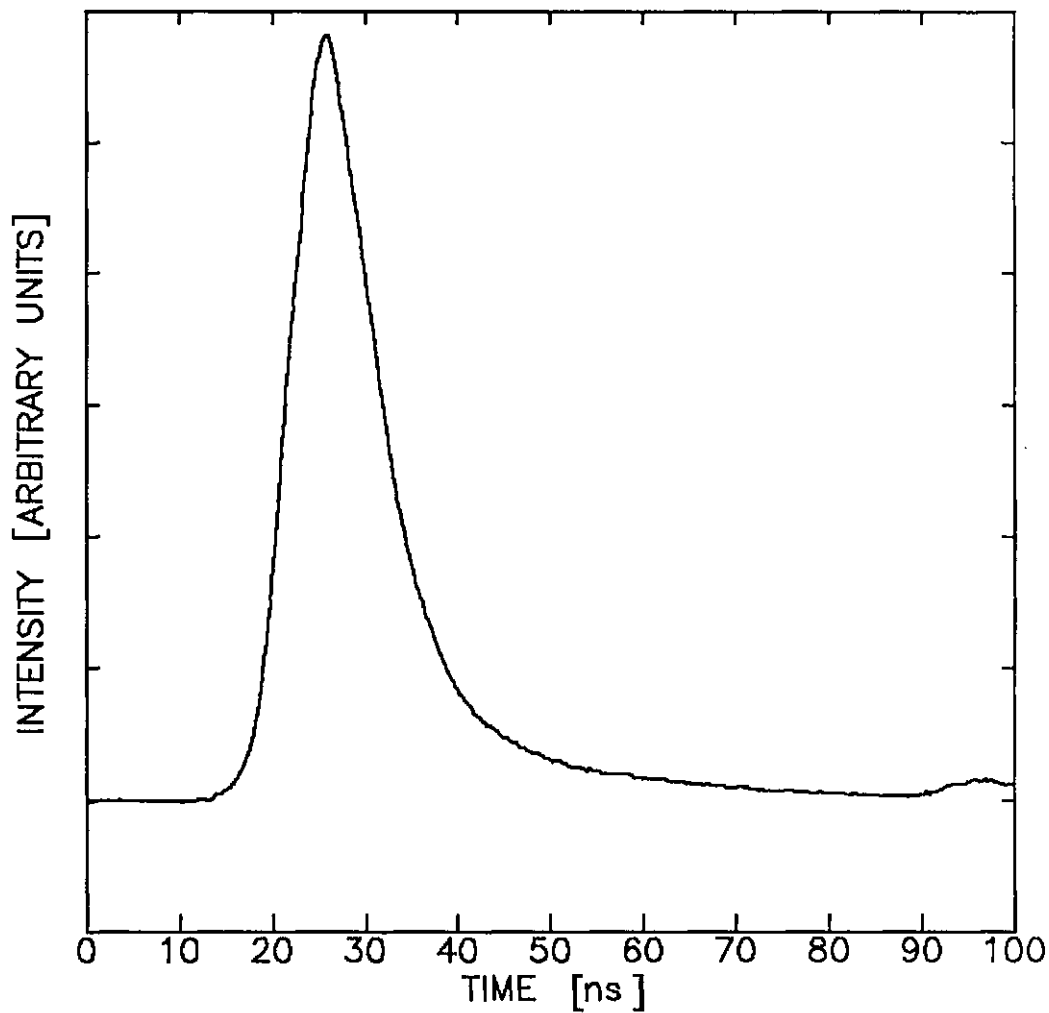


Figure 2-3-1. A typical laser pulse from the DCR-3 ($\lambda = 1064$ nm).

homogenizer was used to diffuse the light and create a relatively uniform intensity distribution. The homogenizer is an acrylic rod with one end highly polished and the other end sanded to give a roughed or hazy appearance. The experimental set-up is shown in figure 2-3-2. The multi-mode radiation incident on the edge of the sample will be approximately 32% reflected which is found by the following equation:

$$R = \left(\frac{1-n}{1+n}\right)^2 \quad (2.3.1)$$

The d term in the exponential of equation 2.2.3 is defined as the distance traversed by the light through the sample. If the incident surface of the sample is not perfect, or if the light is not normally incident (as is the case here with the use of the homogenizer) then the distance travelled in the sample will vary from that used in the derivation. The homogenizer is being used as a waveguide with the added feature of the roughed input surface. Light that is guided will have angles of incidence on the top and bottom of the homogenizer determined by the difference in indices of refraction (1.5 for glass and 1 for air in this case).

Waveguide Characteristics of GaAs

The deviation in the length of light traversal due to non-normal incidence could cause very large errors in the measured absorption length if the angle of incidence (from surface normal) is large (see figure 2-3-3). The numerical aperture of GaAs is very large which allows light, incident at almost any angle, to be coupled into the sample. Fortunately, the index of refraction of GaAs is large compared to air which causes the light to be refracted drastically toward the normal. In other words, the

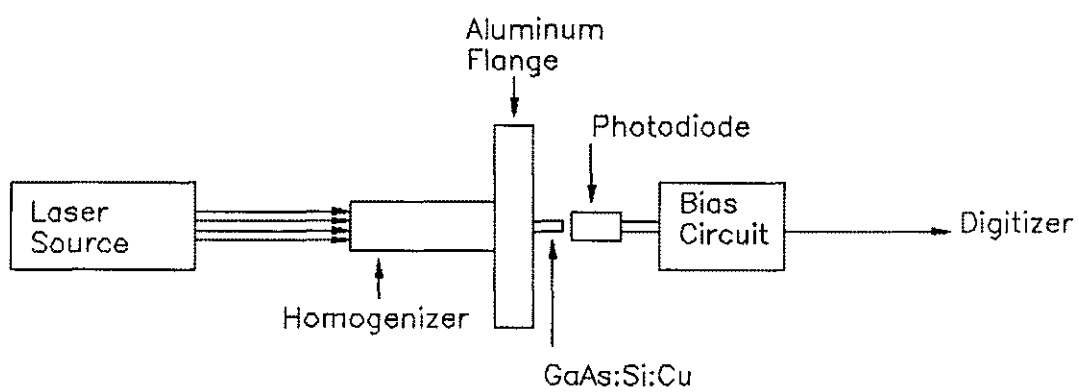


Figure 2-3-2. The experimental set-up for the absorption measurements.

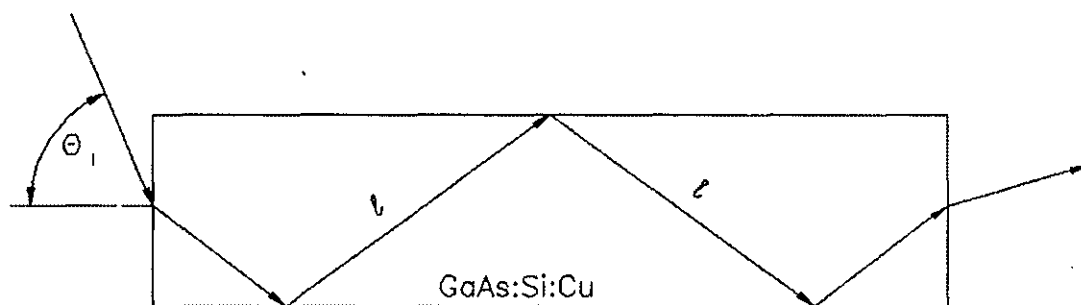


Figure 2-3-3. Traversal of light with non-normal angle of incidence.

angle of incidence inside the sample, at the top and bottom (θ_i in figure 2-3-3), is large. All angles are referenced to the incident surface normals. The index of refraction of GaAs is approximately 3.6 which corresponds to an angle of refraction given by,

$$\sin \theta_r = \frac{n_{air}}{n_{GaAs}} \sin \theta_i \quad (\text{Snell's Law}) \quad (2.3.2)$$

The light is guided to the sample by the homogenizer which has an index of refraction of approximately 1.5 . The minimum angle of incidence that this waveguide can support is:

$$\theta_c = \sin^{-1}(n_{air}/n_{glass}) \approx 42^\circ$$

At the exit end of the homogenizer, light incident at 48° ($90^\circ - 42^\circ$) will be refracted away from the normal. Therefore, the light will be incident on the GaAs surface at an angle greater than 48° . Next, the light will be refracted toward the normal when entering the GaAs. Equation 2.3.2 leads to $\theta_r = 14^\circ$ for a worst case angle of incidence of, say, 60° from the homogenizer. Next, the effective traversal length is calculated as a function of the incidence angle.

$$d_{eff} = N \cdot l \quad (2.3.3)$$

where N = number of reflections, l = hypotenuse length. Using simple geometry, the number of reflections is:

$$N = \frac{d}{t \cdot \tan \theta} \quad (2.3.4)$$

$$l = \frac{t}{\cos\theta} \quad (2.3.5)$$

Using equations 2.3.3, 2.3.4, and 2.3.5, the effective traversal length is then given by:

$$d_{eff} = \frac{d}{\sin\theta} \quad (2.3.6)$$

It is interesting to note that the effective distance is independent of the thickness of the sample. The large numerical aperture of GaAs allows light to be easily coupled to it. Also, the large value of index of refraction causes the light to bend toward the normal in such a way that the effective length of the sample may be approximated by the actual sample length. For instance, a worst case angle of refraction of 14° entering the sample corresponds to an internal angle of reflection of 76° (measured from the normal of the top and bottom surface/air interface). Therefore, the error is approximately 3% in assuming the traversal length to be equal to the actual length of the sample.

Detection of Infrared Radiation

The photodetector must also be carefully selected in order to obtain accurate results. The responsivity of the photodetector to 1064 nm wavelength light must be high enough to generate currents that can be detected. In this case, a 750 MHz, Tektronix 7912AD digitizer was used to measure the current. The photodiode selected was a silicon PIN diode manufactured by RCA with an active area of 0.8 mm^2 , a responsivity of 0.03 A/W, and a rise time of less than 1 ns. A high bandwidth circuit must be used to apply the bias to the sample and measure the

current because of the fast laser pulse used. Figure 2-3-4 shows the photodiode circuit. The circuit is $50\ \Omega$ and the termination of the digitizer is used as the current viewing resistor (CVR). The laser pulse of figure 2-3-1 was measured with this circuit, as any measurements of the temporal behavior of the laser pulses.

Results

The experimental set-up shown in figure 2-3-2 was used to measure the incident and transmitted intensities. The absorption coefficient was subsequently calculated using equation 2.2.4 (transmission). Before reporting the results, it is important to note that the photodiode used in this experiment is very sensitive and saturates easily. In this experiment, the intensity of the transmitted light will change due to repetitive cleavage of the sample, and therefore the photodiode response to such intensity variations must be examined. The effects of photodiode saturation are inaccurately measuring long absorption lengths. Care has been taken to plot the photodiode response as a function of intensity (figure 2-3-5) in order to determine the optimum operating range. As seen in figure 2-3-5, the photodiode must be operated at low intensities to ensure linearity.

The purposes of these measurements center around scaling of the switch and the possible contact geometries that may be used. Also of interest is the effect of copper doping on the absorption characteristics. Gallium arsenide samples with three different doping profiles were used in the absorption experiment. Silicon doped gallium arsenide, delivered from the manufacturer, will be considered first and then compared to copper doped material. In order to study the effect of copper

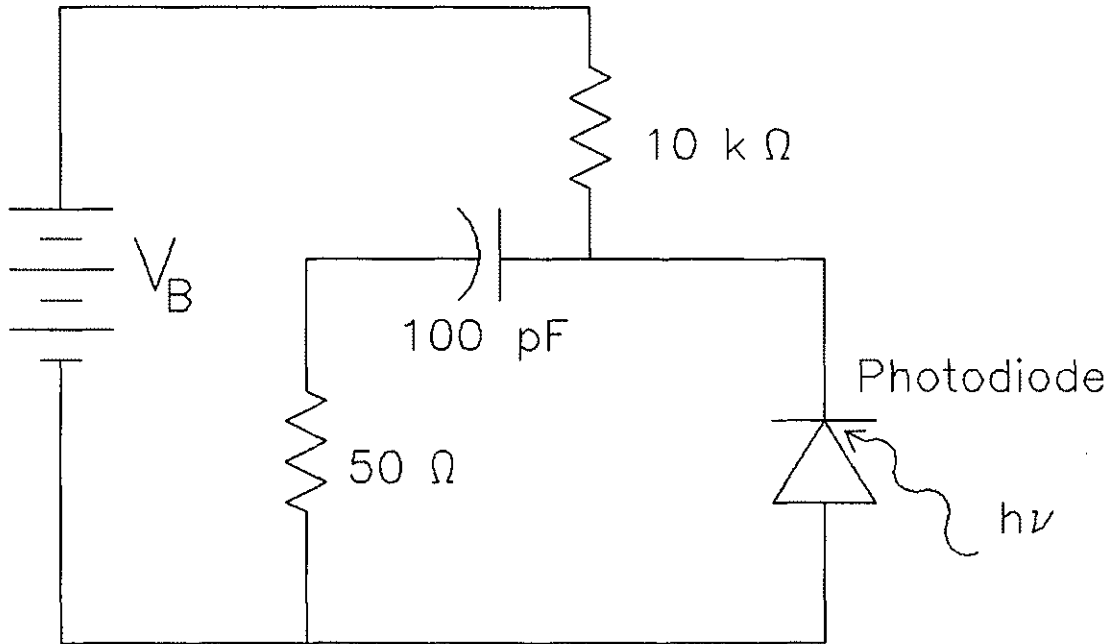


Figure 2-3-4. Photodiode bias circuit.

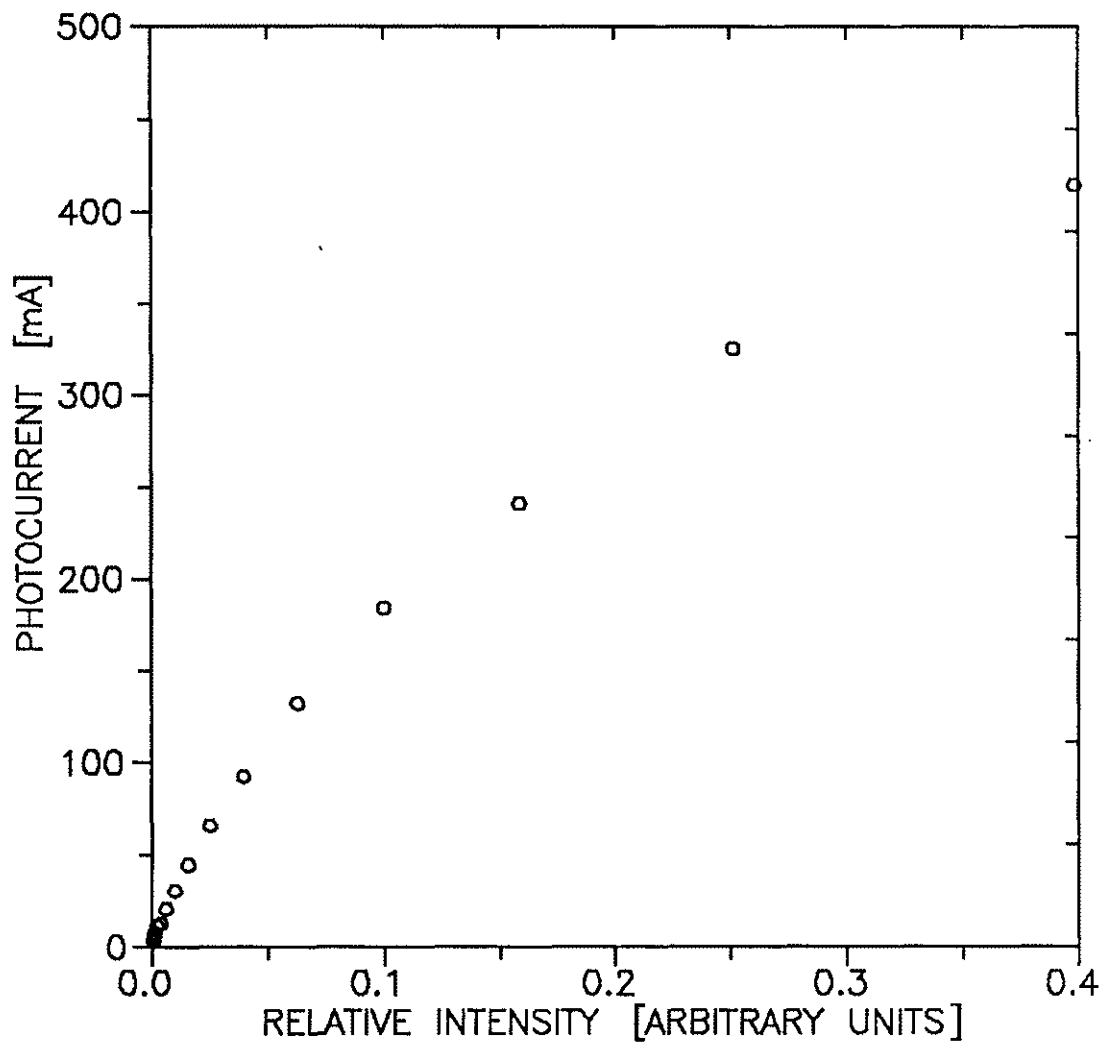


Figure 2-3-5. Photodiode response as a function of laser intensity.

doping, the ideal situation would be to find the absorption depth of silicon doped GaAs and then dope copper into the same sample and measure the absorption depth again. The problem is that the experiment to be used here is destructive to the sample and therefore the same sample cannot be used for absorption measurements before and after copper doping. Samples may, however, be cut from a wafer in strips side-by-side which will effectively ensure that the characteristics of each strip are as similar as possible. One of these strips of GaAs:Si was used directly to measure the absorption depth, and the other was doped with copper before the measurements were made.

The results of the absorption measurements are best displayed in a graph of $\ln(I_T/I_0)$ vs d , where d is the sample length. The slope of this line (using equation 2.2.3) will give the absorption length. The plotted equation is,

$$\ln(I_T/I_0) = -\alpha d + \ln(R-1)^2 \quad (\text{as derived from equation 2.2.4}).$$

The reason for not directly calculating α is experimental error. The gallium arsenide samples must be cleaved a number of times in order to perform this experiment. The incident edge of the sample is usually not perfectly cleaved, and errors occur due to changing the angles of incidence. If the sample is cleaved a number of times and I_T/I_0 is measured each time and plotted against the sample length, the absorption coefficient may be extracted as described earlier. With this method, the errors from the imperfect surfaces should average out. This partially explains the small, but distinguishable, scattering in the data shown in figure 2-3-6. It should be noted that these numbers represent minimum values for the absorption depth. Any leakage of light around the sample, or deviation of the light path from the actual sample length

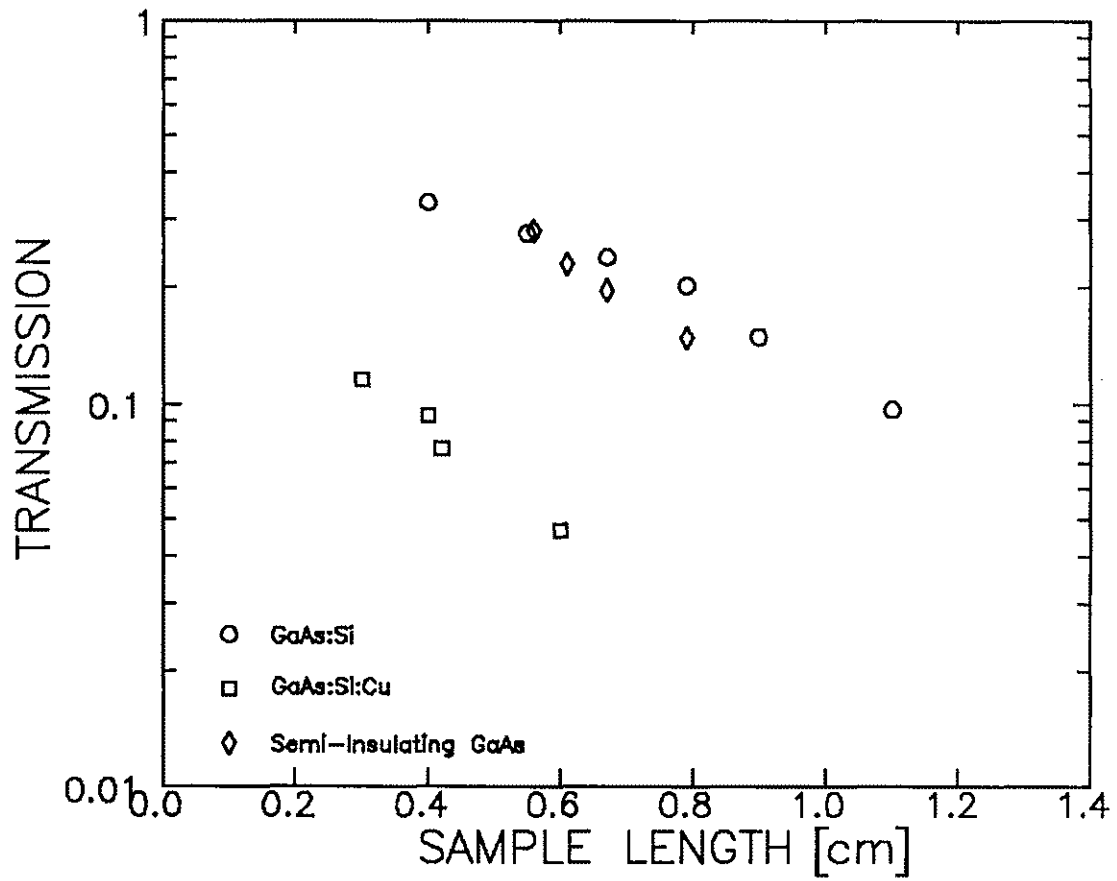


Figure 2-3-6. Results of the absorption measurements for GaAs:Si, GaAs:Si:Cu, and semi-insulating GaAs.

will result in decreasing the measured absorption depth. The data for GaAs:Si shows a break in the curve where the transmission *bends* toward the vertical axis. This is to be expected because multiple internal reflections (higher order terms) become more important as the sample length gets smaller. In this case the absorption coefficient may not be taken as the slope of the line drawn through the data points. Instead, longer sample lengths must be used to ensure an absorption dominant transmission characteristic for which equation 2.2.4 holds. Longer sample lengths create problems experimentally because the sample must be removed after measurements are taken for each sample length. Excess movement of any component of the experimental set-up will cause error in the measured intensity ratio. Short samples allow for easy removal from the apparatus for cleavage and placement back into the bracket (see figure 2-3-2), and therefore the error is less. The intercept in figure 2-3-6 may be used as a *confidence factor* because it should give a real value for the reflection coefficient according to equation 2.2.3. The intercept in figure 2-3-6 gives a reflection coefficient of about 0.45 which is reasonable when considering the experimental error. Therefore the value for the absorption depth for silicon doped, copper compensated gallium arsenide will be reported to be approximately 3 mm based on the slope of the line in figure 2-3-6. The absorption depths for silicon doped gallium arsenide and semi-insulating gallium arsenide are 8 mm each based heavily on average values of the measurements [19]. This appears to be reasonable when compared to the measured value for GaAs:Si:Cu (3 mm) which had a high confidence factor in that the data scatter was minimal and the intercept gave a reasonable value for the reflection coefficient. The copper

doped material obviously has a higher absorption coefficient than GaAs:Si and semi-insulating GaAs as seen in figure 2-3-6.

2.4 SUMMARY

The $1/e$ absorption depths have been measured for GaAs:Si:Cu, GaAs:Si, and semi-insulating GaAs for $\lambda = 1064$ nm and found to be approximately 3 mm, 8 mm, and 8 mm respectively. The information to be extracted from these measurements are summarized as follows:

- Copper controls the absorption of incident laser radiation with a wavelength of 1064 nm in gallium arsenide doped with silicon and compensated with diffused copper. The densities of copper and silicon may be reduced to create longer absorption lengths.
- An absorption depth of 3 mm in GaAs:Si:Cu determines the possible contact geometries that may be employed.
- Geometric scaling of the switch is limited by the depth of penetration of the incident laser light.

A final consideration is that of absorption effects while an electric field is applied to the crystal. This situation is vitally important because the intended uses of the switch are for strong applied electric fields. The Franz-Keldysh effect [15] states that in the presence of an electric field, the tunnelling probability for an electron or hole increases with increasing electric field. For example, the probability of finding an electron in the energy gap decreases exponentially across the barrier

thickness [15]. This photon assisted tunnelling has been used to describe a shift in the absorption edge in GaAs [20]. Other studies have revealed the exponential absorption edge expected from photon assisted tunnelling in slightly over-compensated, p-type, GaAs [21].

CHAPTER 3

DARK CURRENT

3.1 INTRODUCTION

The dark current is defined as the current conducted through the sample due to an applied electric field, and without illumination from an external source such as a laser or electron beam. Application of an electric field and measurement of the resulting current gives rise to I-V curves which may be studied in order to obtain information concerning thermal effects, deep level structure, or injection phenomena in the material of interest. The material of interest here is copper compensated, silicon doped, gallium arsenide. By virtue of the relatively crude method of copper compensation employed to produce the samples used in this thesis, and the fact that gallium arsenide is a very complicated structure, there seems to be little encouragement to those studying the behavior of GaAs:Si:Cu. There is, however, a great deal of information that can be obtained from a few basic effects and some simple approximations. First, thermal effects will be discussed which will involve a simple model for the overheating effect with increasing voltage. The second section involves injection phenomena combined with deep level trapping effects. For this case, some basic theory will be introduced concerning single carrier injection, and then a model based on double injection, and some resulting I-V curves will be

presented. Finally, the theoretical calculations will be compared to experimental results. The focus of the experiments is the production of steady-state I-V curves which will verify the assumptions made in the theoretical calculations.

3.2 THERMAL EFFECTS

Thermal Management is one of the most important limitation of the bulk semiconductor switch concept. In order for a material to be effectively used as a switch, it must be able to hold off high voltages either pulsed or DC. Thermal effects occur when a sufficient DC voltage is applied or when high voltage pulses are applied creating high average power dissipation in the crystal. Before current-voltage measurements are made, it is important that a clear understanding of the basic thermal effects in the crystal are ascertained. When a voltage is applied to the sample, a current conducts creating i^2R losses in the form of heat. At low electric fields, a thermal equilibrium is established between the sample and the environment which stabilizes the current. This current is determined by Ohm's law at low fields, but, as we will see later, the current deviates from Ohm's law at higher fields. It is very important to understand these thermal effects to avoid misinterpretation of data.

Theory

The basic heat equation may be used to describe the overheating in the crystal. This equation appears as,

$$C_m \frac{d\Delta T}{dt} + \Gamma \Delta T - P = 0 \quad (3.2.1)$$

where C_m is the heat capacity, ΔT is the overheating, Γ is the heat loss to the environment, and P is the power loss in the sample. The power loss term can be written as the current multiplied by the voltage, $I \cdot V$. If the resistance is assumed to vary exponentially with the temperature, then the resistance may be written as,

$$R = R_0 e^{\frac{-\Delta T}{T^*}} \quad (3.2.2)$$

where R_0 is the initial resistance of the sample, and T^* is a constant [4,17]. Using this assumption, the characteristic equation (equation 3.2.1) may now be written as,

$$C_m \frac{d\Delta T}{dt} + \Gamma \Delta T - \frac{V^2}{R_0} e^{\frac{\Delta T}{T^*}} = 0 \quad (3.2.3)$$

This is a time dependent equation which may be studied under equilibrium conditions so that equation 3.2.3 reduces to,

$$\Gamma \Delta T - \frac{V^2}{R_0} e^{\frac{\Delta T}{T^*}} \quad (3.2.4)$$

Now, equation 3.2.4 may be simplified by introducing the following two terms:

$$\gamma = \frac{\Delta T}{T^*} \quad (3.2.5)$$

$$k = \frac{V^2}{R_0 \Gamma T^*} \quad (3.2.6)$$

Substituting γ and k into equation 3.2.4 allows the equilibrium expression to be written as,

$$\gamma e^{-\gamma} = k \quad (3.2.7)$$

When the value of k increases to a critical value, the system becomes unstable. The conditions for stability will now be presented. Using,

$$\Delta T \rightarrow \Delta T + \delta T \quad (3.2.8)$$

the characteristic equation may now be written as,

$$\frac{C}{\Gamma} \frac{d\delta T}{dt} + \delta T - \frac{V^2}{R_0 \Gamma} e^{\frac{\Delta T}{T^*}} \frac{\delta T}{T^*} = 0 \quad (3.2.9)$$

Using the time constant $\tau = C/\Gamma$, and the expressions 3.2.5 and 3.2.6, the following relationship is obtained:

$$\tau \frac{d\delta \gamma}{dt} + \delta \gamma - k e^{\gamma} \delta \gamma = 0 \quad (3.2.10)$$

The solution to equation 3.2.10 is exponential with a time constant shown in equation 3.2.11 (λ is the time constant of the instability).

$$\lambda = \frac{\tau}{k e^{\gamma} - 1} \quad (3.2.11)$$

In order for the solution to equation 3.2.10 to be stable, the time constant must be negative, corresponding to a decaying exponential. Therefore, the following expression must be true,

$$ke^{\gamma} < 1 \quad (3.2.12)$$

which leads to the stability criterion [22],

$$\gamma < 1 \quad (3.2.13)$$

A knowledge of the parameters in equation 3.2.3 provides a way to determine if an applied voltage is sufficient to cause a thermal instability and subsequent thermal run-away of the current. Solving equation 3.2.3 is possible but not necessary in this case, because the stability of the system can be determined without numerical analysis. Figure 3-2-1 shows the expected current-voltage relationship (solid line) with broken lines indicating the thermal stability curve (equation 3.2.7). Notice that the I-V curve deviates from Ohm's law as the voltage increases, but the current is still stable until the threshold voltage, V_{th} , is reached.

Another calculation that may be constructive here is that of the thermal conduction in the sample. Fourier's heat equation describes this situation and is given as,

$$C\rho \frac{\partial T}{\partial t} = \nabla \dot{q} - \kappa \nabla^2 T \quad (3.2.14)$$

where ρ is the crystal density, C is the specific heat, and k is the lattice thermal conductivity. This equation allows us to get an order of magnitude approximation for the time required for the sample to reach thermal uniformity throughout the volume of the crystal. This is accomplished by replacing the time derivative in equation 3.2.14 by $1/\tau$ and the spatial derivative by $1/L$. The resulting expression

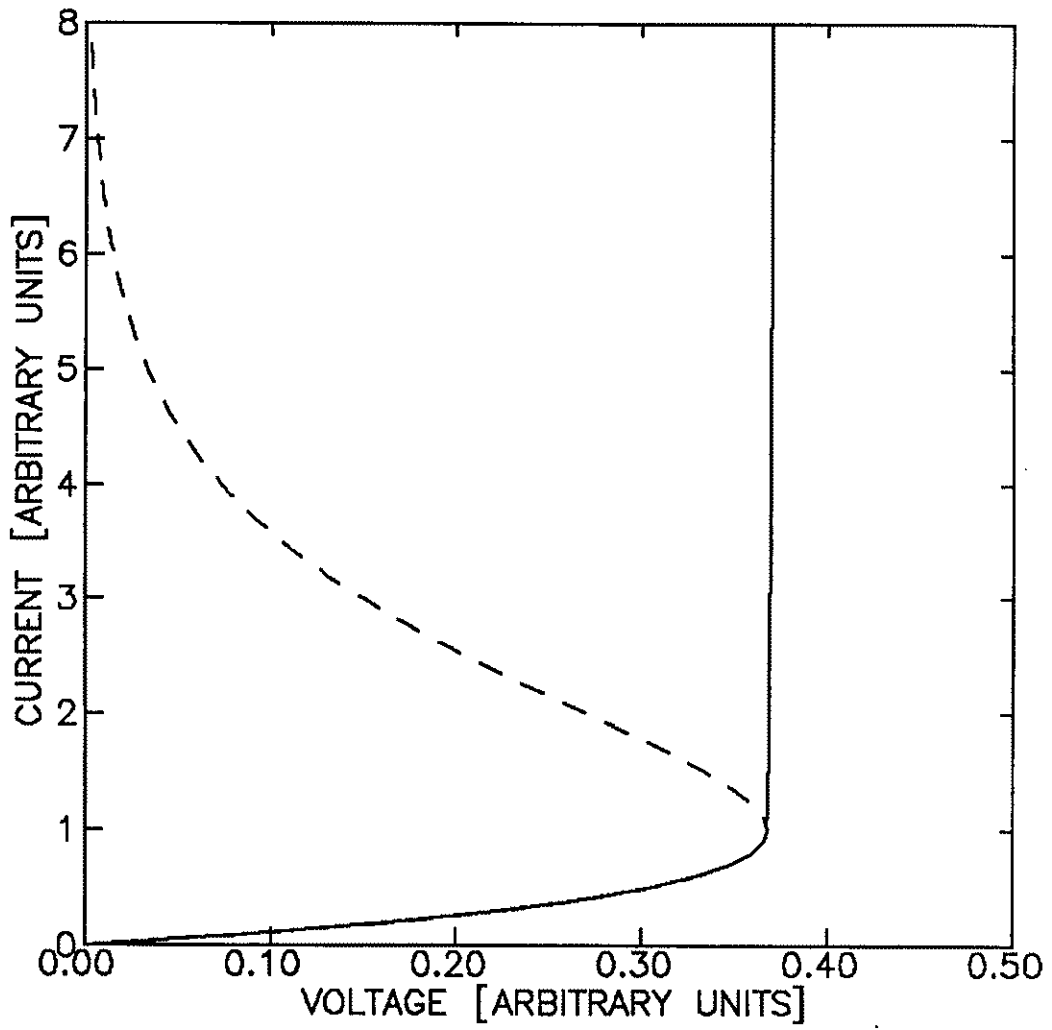


Figure 3-2-1. Expected I-V curve (solid line) and the thermal stability curve (dashed line).

can be solved for τ , the approximate time for thermal energy to conduct from the contacts to the edge of the sample.

$$\tau = \frac{C\rho L^2}{\kappa} \quad (3.2.15)$$

The values for the crystal density, specific heat, and lattice thermal conductivity have been given by Blakemore to be 5.32 g/cm³, 0.327 J/g·K, and 0.5 W/cm·K respectively [23]. Using these values, the approximate time of thermal conduction (equation 3.2.15) is 35 ms for a distance of 0.1 cm. This result is important because it may become necessary to know if only the volume between the contacts, or the entire volume of the sample should be considered. The following experiments will be performed to find the values for Γ and T^* .

Experiments and Results Related to the Thermal Model

Steady state current-voltage curves may be generated by simply applying a voltage, waiting until the current stabilizes, and then measuring the current. In this experiment, a Keithly electrometer was used to apply the voltage and measure the resulting current for voltages up to 100 volts and currents of up to 3 mA. Voltages higher than 100 V were applied by an external source (Bertram). The physical properties of the samples used in this experiment are summarized in table 3-1. As the voltage was increased across sample 1297-14-A10, a break point was observed at which the current became unstable. This may be due to trap filling, thermal effects, or both. Similar break points were observed in semi-insulating GaAs [5], which were

Table 3-1. Material parameters for three gallium arsenide samples.

Sample Name	Si Density [cm ⁻³]	Cu Diffusion Temperature [°C]	Thickness [cm]	Contact Area [cm ²]	Resistivity [Ω·cm]
1297-10-A5	4.7 x 10 ¹⁶	565	0.058	0.071	1 x 10 ⁵
1297-10-A9	4.7 x 10 ¹⁶	561	0.061	0.050	5 x 10 ⁶
1297-10-A10	4.7 x 10 ¹⁶	562	0.066	0.050	2 x 10 ⁶

considered to be due to injection phenomena and trap filling. A thermal model would predict the break points to occur at a higher voltage as the temperature is reduced or the thermal environment is improved, which is clearly not the case here. This procedure of changing the temperature and environment was done using sample 1297-14-A10, and the results are shown in figure 3-2-2. There are some thermal effects governing the break point which moved to higher voltages as the temperature decreased. Placing the sample in an environment that is much more heat conductive than air also caused the break point to shift to higher voltages which again leads to the conclusion that thermal effects are causing the instability. It is constructive at this time to define the thermal model presented earlier quantitatively. In order to do so, a knowledge of the parameters in equation 3.2.3 is needed. The values for the specific heat, C , the voltage, V , and the initial resistance, R_0 , are constants. The heat loss to the environment, Γ , and the temperature, T^* , are to be found experimentally. The first experiment will be designed to find the value for Γ . To do this, it is necessary to apply a small voltage to the sample so that with a high initial resistance, the third term in equation 3.2.3 may be neglected. The resulting equation is given as,

$$C \frac{d\Delta T}{dt} = -\Gamma \Delta T \quad (3.2.16)$$

From equation 3.2.16, the time constant is given as C/Γ . This situation can be produced experimentally by applying a small voltage to a sample in air or vacuum, heating the sample to a high temperature, removing the heat, and then recording the temporal decay of the current. This experiment has been done using sample

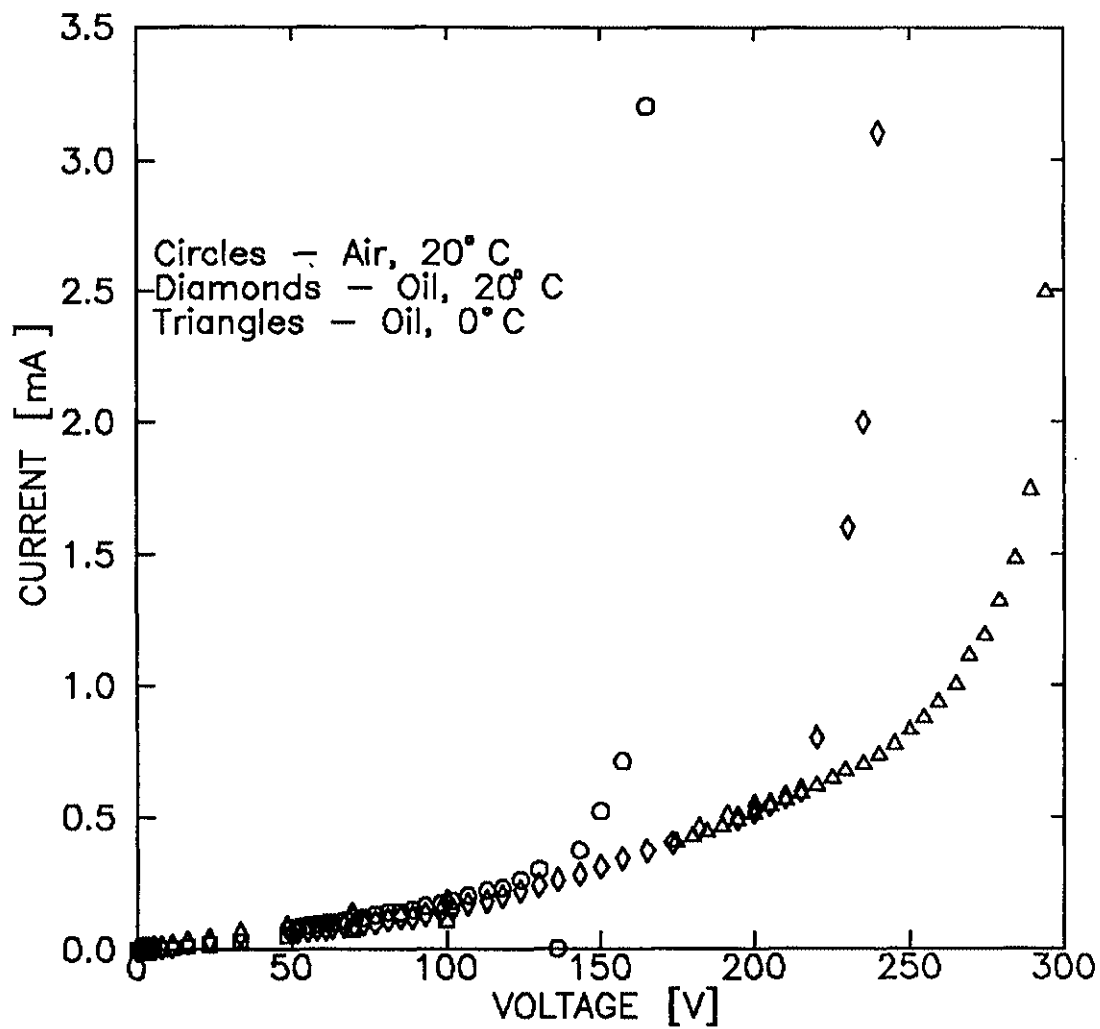


Figure 3-2-2. Current-Voltage curves for sample 1297-14-A10 in different thermal environments.

1297-10-A5, and the results are shown in figure 3-2-3. The current starts at a high value and then decays exponentially to a steady state value I_p , which has been subtracted from the data in figure 3-2-3. Plotted on a semi-log plot, a straight line may be drawn through the data and the slope taken as the time constant. In this case, the time constant was 108 seconds. Using the value of C found earlier, the value for Γ becomes,

$$\frac{C}{\Gamma} = 108s \rightarrow \Gamma = \frac{C}{108s} = \frac{327 \frac{W \cdot s}{kg \cdot K}}{108s} = 3.03 \frac{W}{kg \cdot K} \quad (3.2.17)$$

It should also be noted that the derivation shown earlier concerning the estimate of the time constant for heat flow from the contacts of the sample to the edges of the sample revealed a time constant of 35 ms. This time is much less than the 108 s time constant of figure 3-2-3 and therefore the entire volume of the sample must be considered.

The next experiment involves finding the value for T^* . This has in effect already been done since an evaluation of $R(T)$ simply requires a measurement of the current-voltage curves at different temperatures. This has been done by others [5,11].

Pulsed Voltage

Pulsed voltage experiments were also performed in order to determine the temporal development of the dark current. Semi-insulating gallium arsenide has been shown to exhibit a rapid transition in current with small increments in voltage [5]. The double injection model seems to describe this effect very nicely. The results

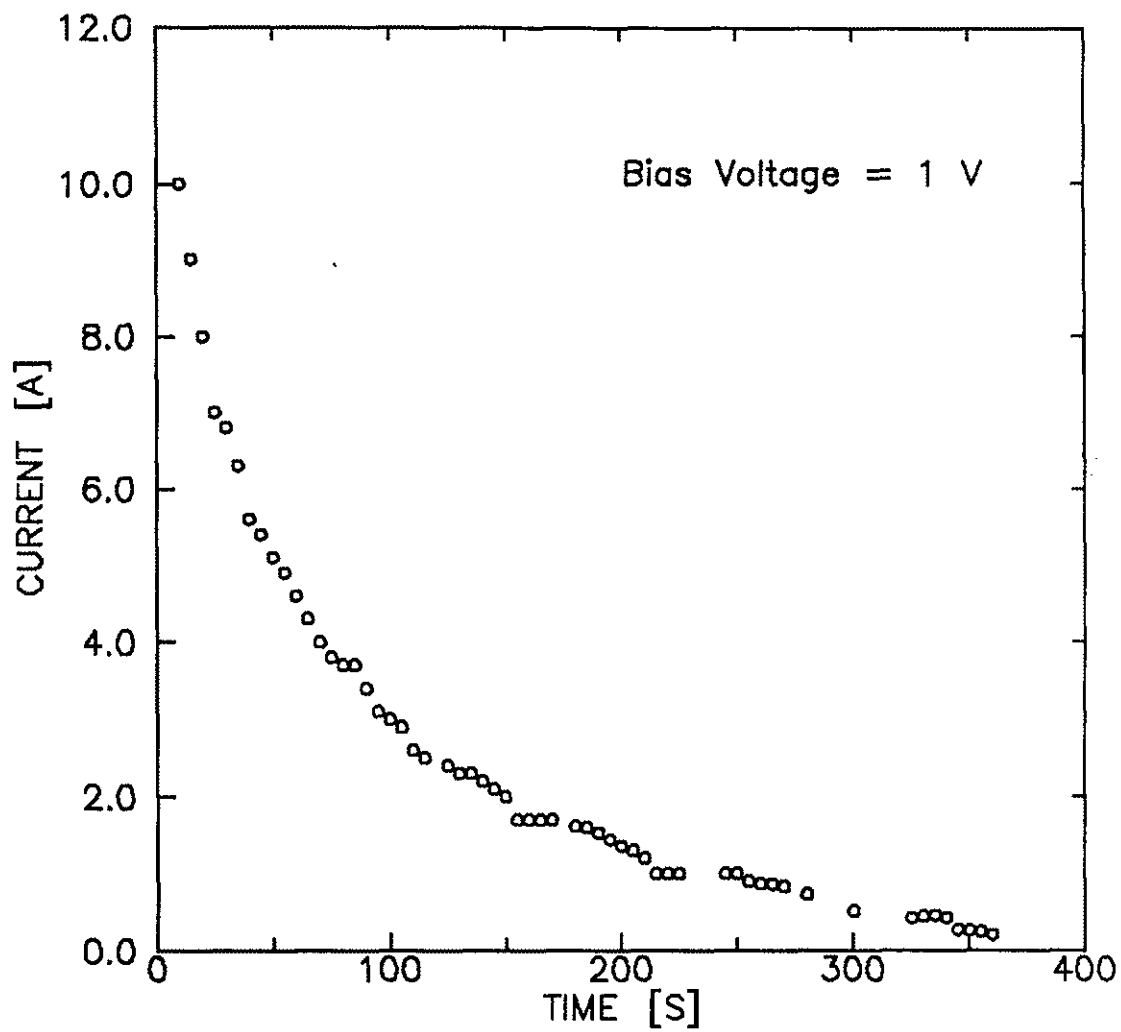


Figure 3-2-3. The temporal decay of the current after a heat source was removed. The sample environment was air.

have shown a temperature dependence that excludes thermal effects. Copper compensated gallium arsenide has shown a thermal run-away of the current (with a DC voltage) before any transition due to double injection. If, however, the applied bias voltage is pulsed, then much higher voltages may be applied and a possible temporal development of the dark current may take place. Using a hard tube pulser, bias voltages of up to 400 V (10 kV/cm) have been applied to sample 1297-10-A5 with no temporal development of the dark current over a 400 ms pulse duration.

3.3 DOUBLE INJECTION

Current injection into solids has been studied extensively [24-27]. The injection of one carrier type leads to the space charge limited current flow and

$$J = \frac{9}{8} \epsilon \mu \frac{V^2}{L^3} \quad (3.3.1)$$

the $J(V)$ relationship shown in equation 3.3.1. This equation is known as the trap-free square law, and has been studied with respect to semi-insulating gallium arsenide [5,24]. This square law is valid in a solid with no deep traps, which is obviously not the case with gallium arsenide. Lampert has shown that equation 3.3.1 is valid in a solid with traps after these traps are filled [24]. Double injection creates an electron-hole plasma introducing both carrier types into the semiconductor through the contacts. In this case, space charges may be neutralized and the current is no longer space charge limited. The mechanism of recombination, however, becomes the current limiting factor. Consider the injection of electrons at the cathode ($x=0$) and holes injected at the anode ($x=L$). If diffusion currents are

neglected (which is valid for long samples $> 1 \mu\text{m}$), the current equations for electrons and holes are,

$$J_p = qp\mu_p E \quad (3.3.2)$$

$$J_n = qn\mu_n E \quad (3.3.3)$$

The drift and diffusion equations may be derived starting with the Boltzmann equation and using Maxwell's equations. Neglecting the effects of the magnetic field created by a current in the sample, the following relations may be used:

$$\epsilon_0 \epsilon_r \nabla \cdot E = \rho \quad (3.3.4)$$

$$\nabla \times E = 0 \quad (3.3.5)$$

Equations 3.3.6, 3.3.7, and 3.3.8 may be solved to determine the electrical characteristics of the material (neglecting diffusion currents).

$$\frac{\partial n}{\partial t} + \frac{\partial}{\partial x}(v_n(E) n) = -\frac{n}{\tau} \quad (3.3.6)$$

$$\frac{\partial p}{\partial t} + \frac{\partial}{\partial x}(v_p(E) p) = -\frac{p}{\tau} \quad (3.3.7)$$

From equation 3.3.4, Poisson's equation may be found,

$$\frac{\epsilon_0 \epsilon_r dE}{q dx} = p - n + \delta\rho \quad (3.3.8)$$

The $\delta\rho$ term in equation 3.3.8 accounts for fixed charge in the material, by following the change in density of trapped carriers. A deep trap enters the problem by effecting the carrier lifetimes, and therefore the recombination processes, and by the amount of charge associated with the level which is accounted for in Poisson's equation. Poisson's equation will not be substantially perturbed by the change in

charge density at the deep level unless the density of deep traps is large compared to the thermal densities of free carriers. Therefore, at least one deep center with a substantial trapped charge density (δp for holes) must be considered here. The lifetimes of injected carriers changes during injection due to the filling of the deep centers which can cause current instabilities [28]. Particle conservation requires the steady state recombination rate densities to be,

$$r_n = \frac{1}{q} \frac{dJ_n}{dx} = -\frac{n}{\tau} \quad (3.3.9)$$

$$r_p = -\frac{1}{q} \frac{dJ_p}{dx} = \frac{p}{\tau} \quad (3.3.10)$$

The double injection, then, is strongly coupled to recombination kinetics in conjunction with the trapping behavior of the deep levels in the bandgap. Specifically, the filling of deep traps causes current instabilities.

Current instabilities caused by negative differential conductivity (ndc) lead to another phenomenon called *filament formation* [25,29]. A current filament can be formed when an instability such as ndc is observed in the I-V curve. If there is any slight field enhancement due to contact edges or inhomogeneities, then that will be the most likely spot for the formation of a filament. Cross-sectional areas as small as 10^{-3} cm^2 have been reported for double injection current filaments in GaAs [30].

Modeling the I-V Characteristics

A computer simulation of the electrical characteristics of the material based on the previous discussion has been developed [31]. This model of the switch has

been used to show the validity of the double injection theory for semi-insulating gallium arsenide, with one deep level, in the dark and under illumination [31,32]. The purpose of this section is to demonstrate the effectiveness of the model with respect to silicon doped, copper compensated, gallium arsenide subject to an electric field with and without illumination from a constant source. The material parameters that have been used are summarized in table 3-2. The simulation number will be used to identify the different simulations when they are compared later. The capture cross sections for electrons and holes at Cu_B , Cu_A , and EL2 are 8×10^{-21} , 3×10^{-14} , 2.7×10^{-17} , 4×10^{-15} , and 8×10^{-13} , 3×10^{-16} cm^2 respectively [12,33]. The first step is to study the effect of a copper level located 0.44 eV from the valence band. Simulation #1 gives the current-voltage relationship shown in figure 3-3-1 (top). At around 200 V, in the simulation, the current begins to saturate at $10 A/cm^2$ the curve changes slope and negative differential conductivity (ndc) is observed. It should be noted that this simulation only accounts for one level in the bandgap; Cu_A and EL2 levels are not considered in the calculation. Simulation number two (figure 3-3-1 (bottom)) corresponds to a more strongly p-type sample, which shows a similar voltage hold-off to the closely compensated sample. In simulations #1, and #2, negative differential conductivity was observed and will be discussed in more detail when corresponding experimental results are presented. Negative resistance in GaAs has been reported elsewhere [4,24,25,27,29].

A more realistic situation than that in simulations #1 and #2 is created when more energy levels are introduced into the calculations. The model has therefore been augmented with two additional levels known as EL2, and Cu_A , which are known

Table 3-2. Material parameters used in the simulations.

Simulation Number	Resistivity	Trap Energy Levels	Trap Densities $\times 10^{16}$	Free Hole Density
[#]	$[\Omega \cdot \text{cm}]$	[eV]	$[\text{cm}^{-3}]$	$[\text{cm}^{-3}]$
		$\text{Cu}_B, \text{Cu}_A, \text{EL2}$	$\text{Cu}_B, \text{Cu}_A, \text{EL2}$	
1	2.16×10^6	0.44, -, -	8, 0, 0	7.2×10^9
2	1.56×10^4	0.44, -, -	8, 0, 0	1.0×10^{12}
3	3.80×10^7	0.44, 0.14, 0.8	1, 1, 0.5	4.10×10^8
4	2.75×10^4	0.44, 0.14, 0.8	1, 1, 0.5	5.69×10^{11}
5	4.08×10^7	0.44, 0.14, 0.8	1, 5, 0.5	3.82×10^8
6	1.07×10^4	0.44, 0.14, 0.8	1, 5, 0.5	1.46×10^{12}

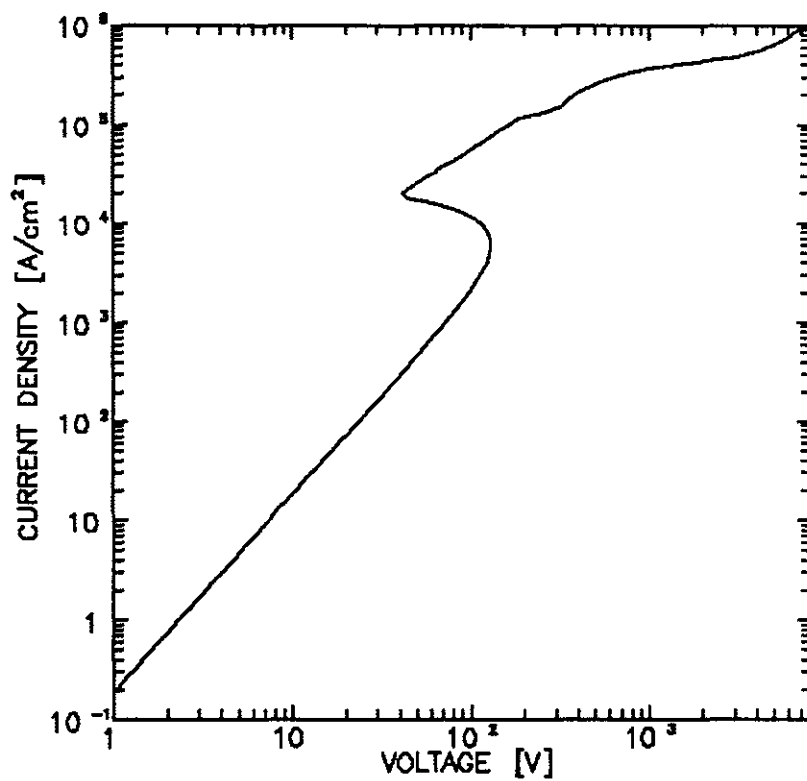
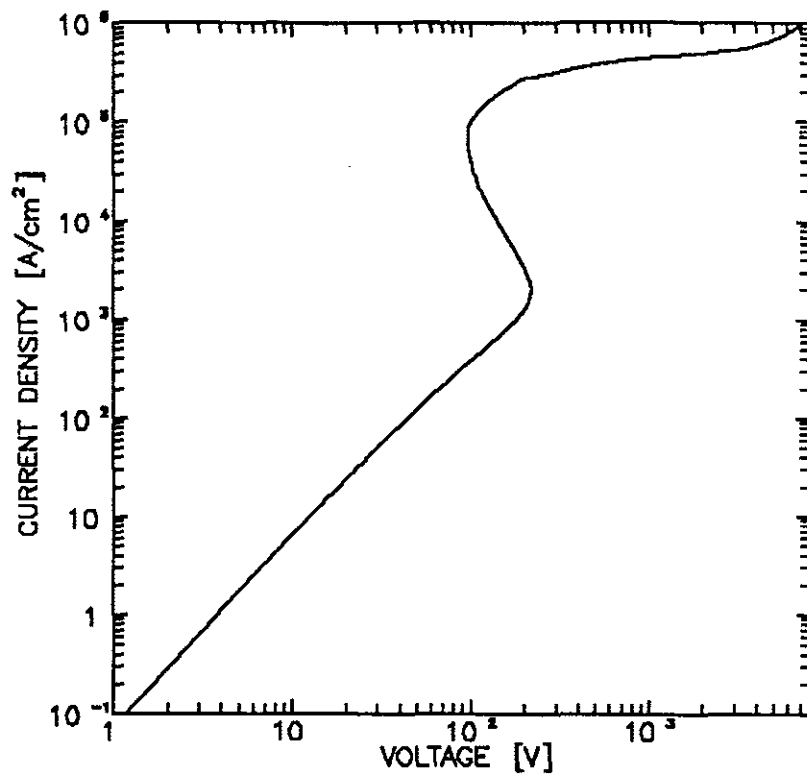


Figure 3-3-1. The I-V curves for simulations #1 (top) and #2 (bottom).

to exist in GaAs [12,35]. Concentrations and the activation energies of these centers are known to some degree. The capture cross-sections for electrons and holes for Cu_A were obtained from Lang [33]. With the introduction of these levels into the bandgap, simulations #3, and #4 were acquired. Simulation #3 was run with a partition (ratio of Cu_A density to Cu_B density) of 1, which resulted in the $J(V)$ curve of figure 3-3-2 (top). A study of the effect of the partition on the dark conductivity of the material was done by Mazzola [11]. In fact, Ohm's law is obeyed for voltages in excess of 1000 volts which was not the case in the first two simulations. Next, the effect of changing the free hole density (ie. creating a strongly p-type sample) was examined. The effect was that the voltage collapse occurred at approximately the same voltage as before (simulation #4 - figure 3-3-2 (bottom)). After the collapse to about 100 V and an increase in current density of two orders of magnitude, the voltage settles at 300 V as the current increases. If the partition is changed according the experimental results from PICTS measurements [35] where a partition greater than unity was observed, then the $J(V)$ curve of figure 3-3-3 (top) is generated (simulation #5). This curve is for a closely compensated, slightly p-type material. Increasing the hole concentration and thus decreasing the resistivity, produced the $J(V)$ curve for simulation #6 shown in figure 3-3-3 (bottom). In this curve a minimum voltage of about 30 V is observed at a current of greater than $5 \times 10^3 \text{ A/cm}^2$.

The current-voltage characteristics may also be studied under irradiation using this model. Simulations #3, and #4 may be presented along with the results using sources of 10^{21} and $10^{18} \text{ cm}^{-3}\text{s}^{-1}$ respectively (see figure 3-3-4). In each case, the dark

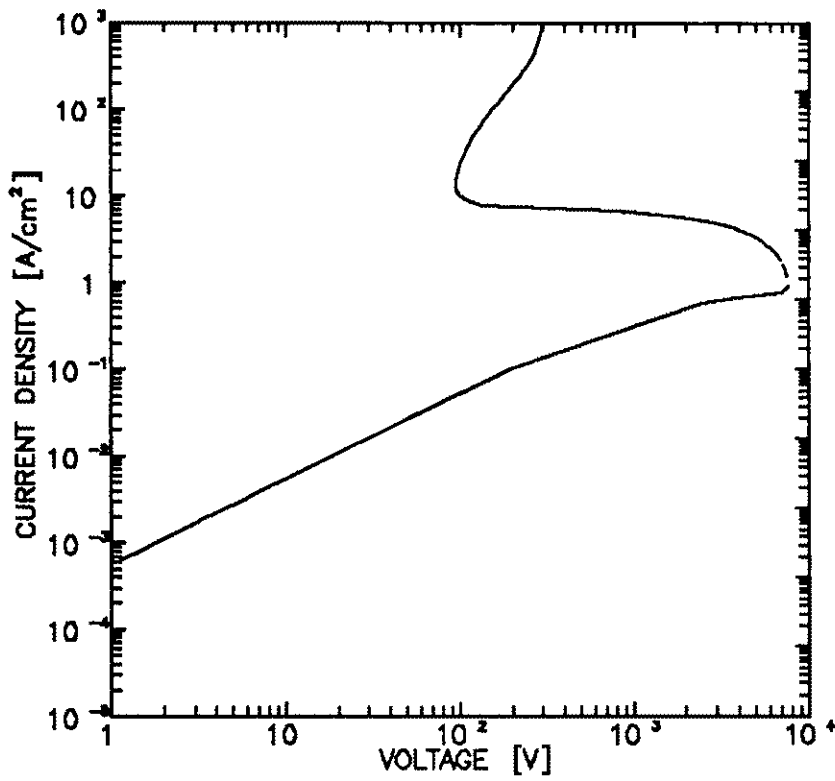
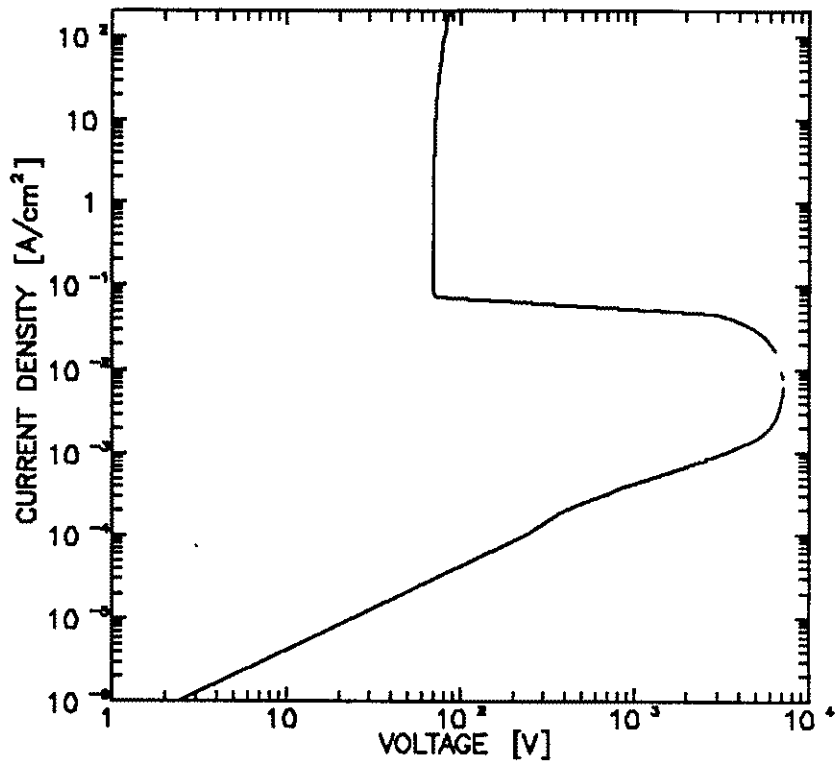


Figure 3-3-2. The I-V curves for simulations #3 (top) and #4 (bottom).

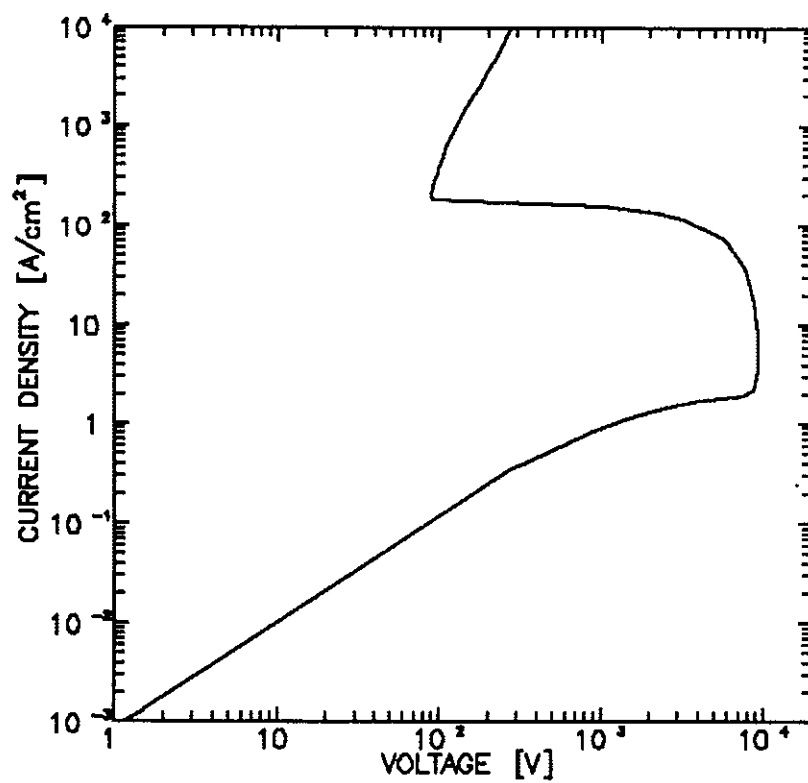
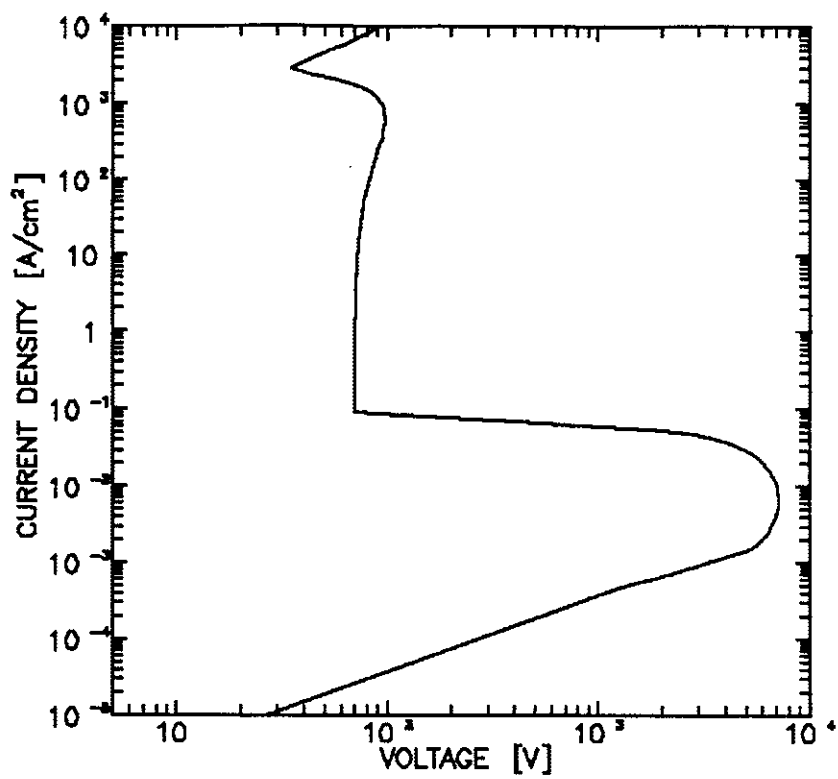


Figure 3-3-3. The I-V curves for simulations #5 (top) and #6 (bottom).

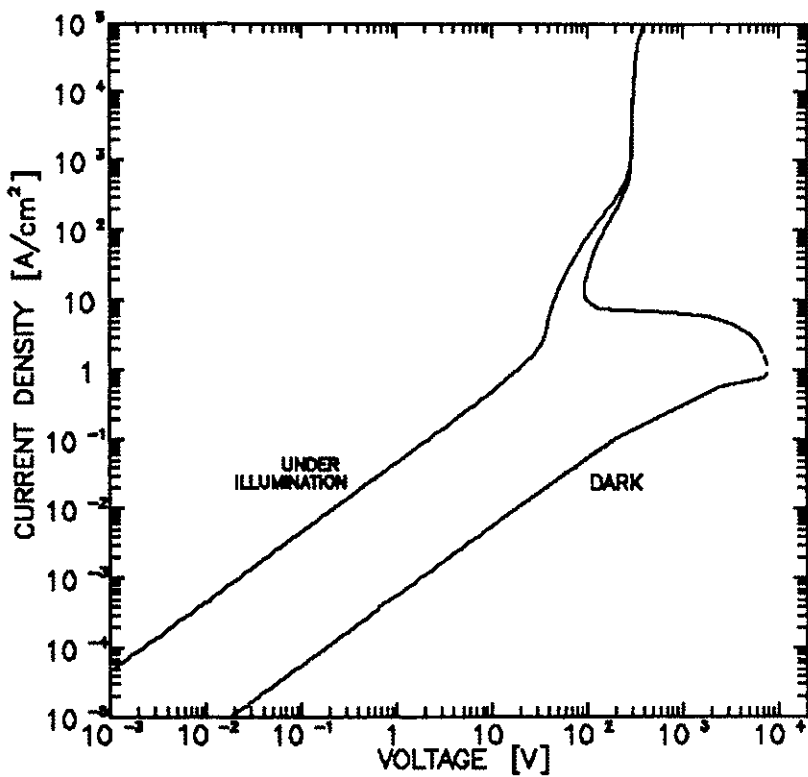
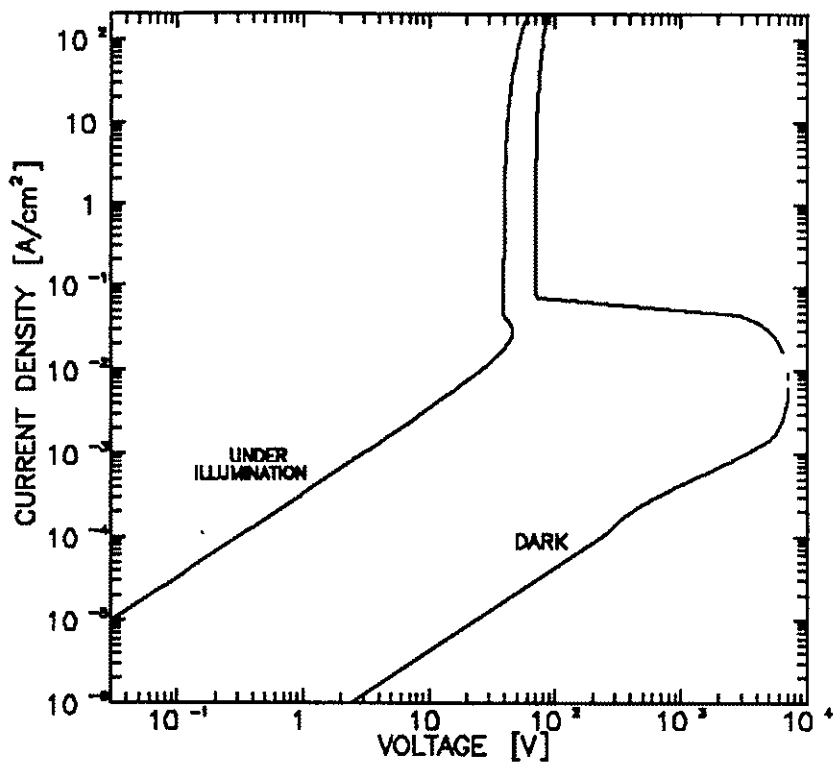


Figure 3-3-4. The I-V curves for simulations #3 (top) and #4 (bottom) under irradiation.

current curve and the illumination curve meet after the collapse of the voltage and an increase in the current is observed in the dark I-V relationship (ndc). This trend will also be discussed in greater detail later.

The important results of the simulations are that the current controlled negative resistance is observed when deep acceptor levels are added, and that the J(V) curves can be adjusted by changing the densities and cross sections. For example, the maximum voltage hold-off was increased from 6 kV to 8 kV by decreasing the ratio of Cu_A to Cu_B density from 5 to 1. Also, the minimum voltage drop after the onset of ndc was reduced by a factor of two (in many cases) by reducing the free hole density a few orders of magnitude.

3.4 EXPERIMENTS AND RESULTS

The major issue to be addressed here is the negative differential conductivity. The first experiments to be performed are measurements of the steady state dark current characteristics without the intrusion of thermal effects. These thermal effects have been explored in section 3.2 and they may be neglected if the voltage is applied for a sufficiently short time. The experiments will be carried out using voltage pulses with either a 40 μ s, 300 ns, or 600 ns pulse width. The current-voltage relationship will then be extracted at a fixed time during the pulses.

The double injection model displayed a negative differential conductivity at high voltages. The 40 μ s pulse was applied to sample 1297-10-A5 and the resulting voltage and current waveforms are shown in figure 3-4-1, and it should be noted that the applied voltage corresponds to an average electric field of 32 kV/cm. The

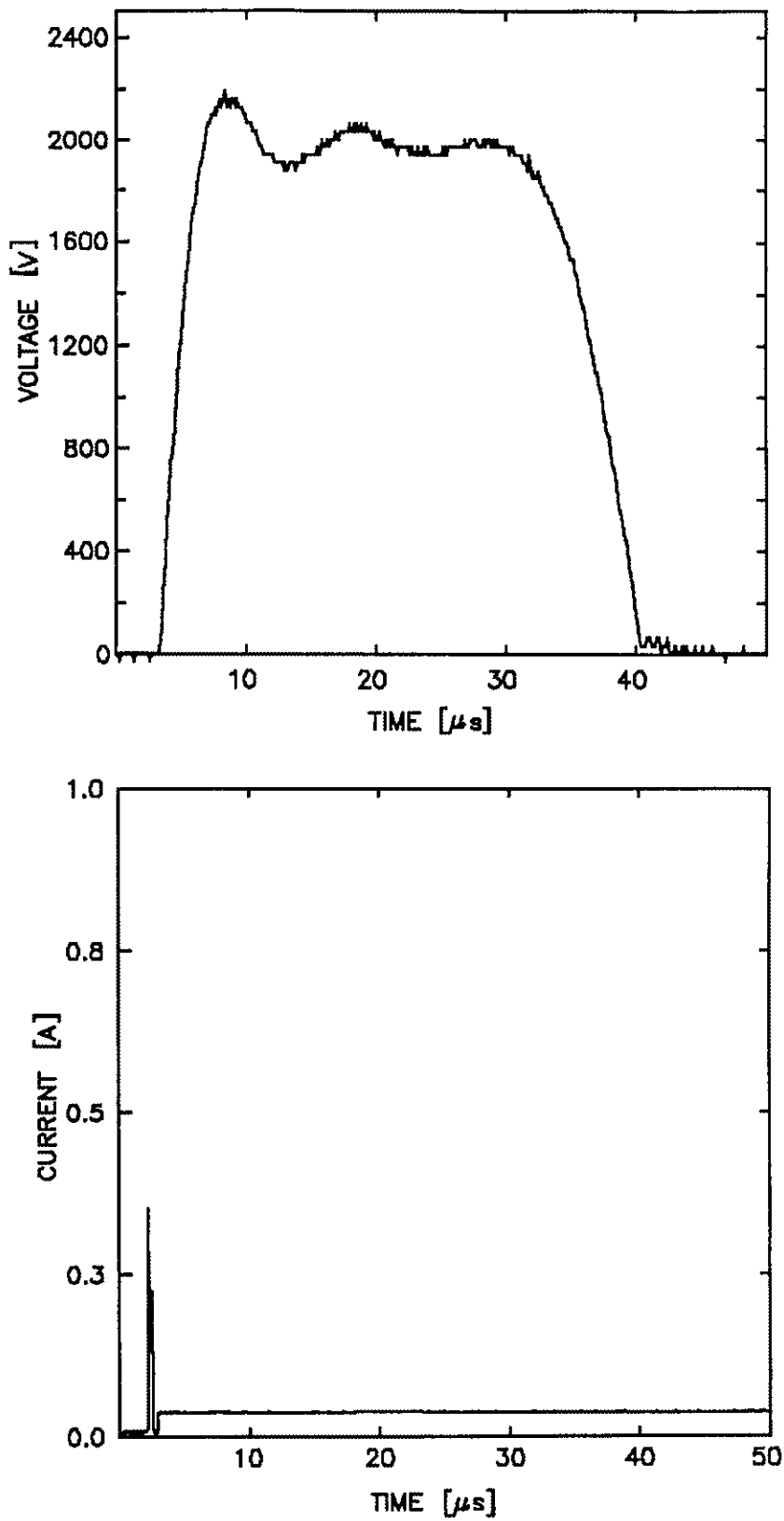


Figure 3-4-1. Sample 1297-10-A10 current waveform resulting from an applied bias voltage of 40 μs duration.

current-voltage relationship does not show the rapid transition that was expected at the higher voltages. The reason is believed to be that the material in this case is strongly p-type. The theoretical model predicted that the maximum voltage that the crystal could hold off before the onset of ndc was adjustable based on the doping profile within the material.

The next step was to investigate the behavior of a closely compensated, or slightly p-type, sample. Two such samples were created and named 1297-10-A9, and 1297-10-A10 whose characteristics were displayed in table 3-1. Pulses from the PFN were applied to sample 1297-10-A10, and at a voltage of just over 800 V (7 kV/cm), a dramatic effect was observed. The current rapidly transitioned from a few hundred milli-amperes up to tens of amperes. This sudden current development was also accompanied by a voltage collapse across the sample to approximately 300 V which corresponds to previous lock-on electric fields [19]. The collapse of the voltage and corresponding increase in current is evidence of negative differential conductivity. The sample was partially destroyed during this experiment due to a narrow *hole* that was burned through the sample at the edge of the contacts. Inspection of the sample revealed a small black spot on the edge of one contact and a corresponding spot on the opposite contact which is strong evidence that a filament was formed when the voltage collapsed. The location of the filament is believed to be due to field enhancement at the edges of the contacts. This same behavior was observed in sample 1297-10-A9.

The sample destruction occurred after the current development and approximately 5 μ s with the field applied. The samples were saved by cleaving the

burned part of the samples and re-using the rest with an applied voltage pulse that was less than 5 μ s. In order to test the samples with lower energy input, the circuit shown in figure 3-4-2 was constructed in order to generate either a 300 ns or 600 ns pulse. The short pulse is generated using a 100 foot, RG-8, 52 Ω , cable, and the longer pulse uses two 100 foot cables connected together. The diagnostics involved 750 MHz and 500 MHz Tektronix Digitizers in conjunction with 50 Ω RG-58 cable to measure the current and voltage respectively. The sample was mounted in a 50 Ω microstrip line in order to maintain the circuit bandwidth integrity. To prevent surface flash-over, the 50 Ω microstrip line with sample was mounted in a quartz pressure chamber filled to about 25 psi SF₆.

The circuit of figure 3-4-2 was used to apply a 600 ns pulse to sample 1297-10-A5. At applied voltages of greater than 2 kV (32 kV/cm), the onset of negative differential conductivity was observed. The voltage collapsed to a value of 600 V, and the current transitioned from a few tens of milli-amperes to tens of amperes. The current development may be observed in a series of current waveforms shown in figure 3-4-3, where the onset time decreases and the magnitude of the current increases as the voltage increases from *a* to *b*. The current waveform for the curve labeled *a* in figure 3-4-3 is shown in figure 3-4-4 with the corresponding voltage waveform. The current development onset time may be defined as the time at which the current transitions into the ampere range. Zero onset time implies that the current development occurs immediately after the peak voltage is reached. This onset time decreases with increasing electric field as shown in figure 3-4-5. The negative differential conductivity observed with the model in section 3.3 is also

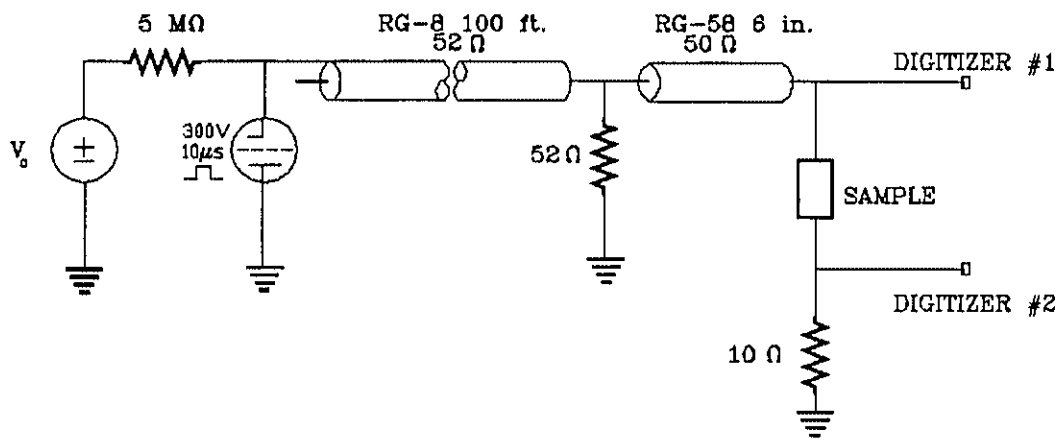


Figure 3-4-2. The transmission line pulser circuit used to apply 300 ns and 600 ns pulses to the samples.

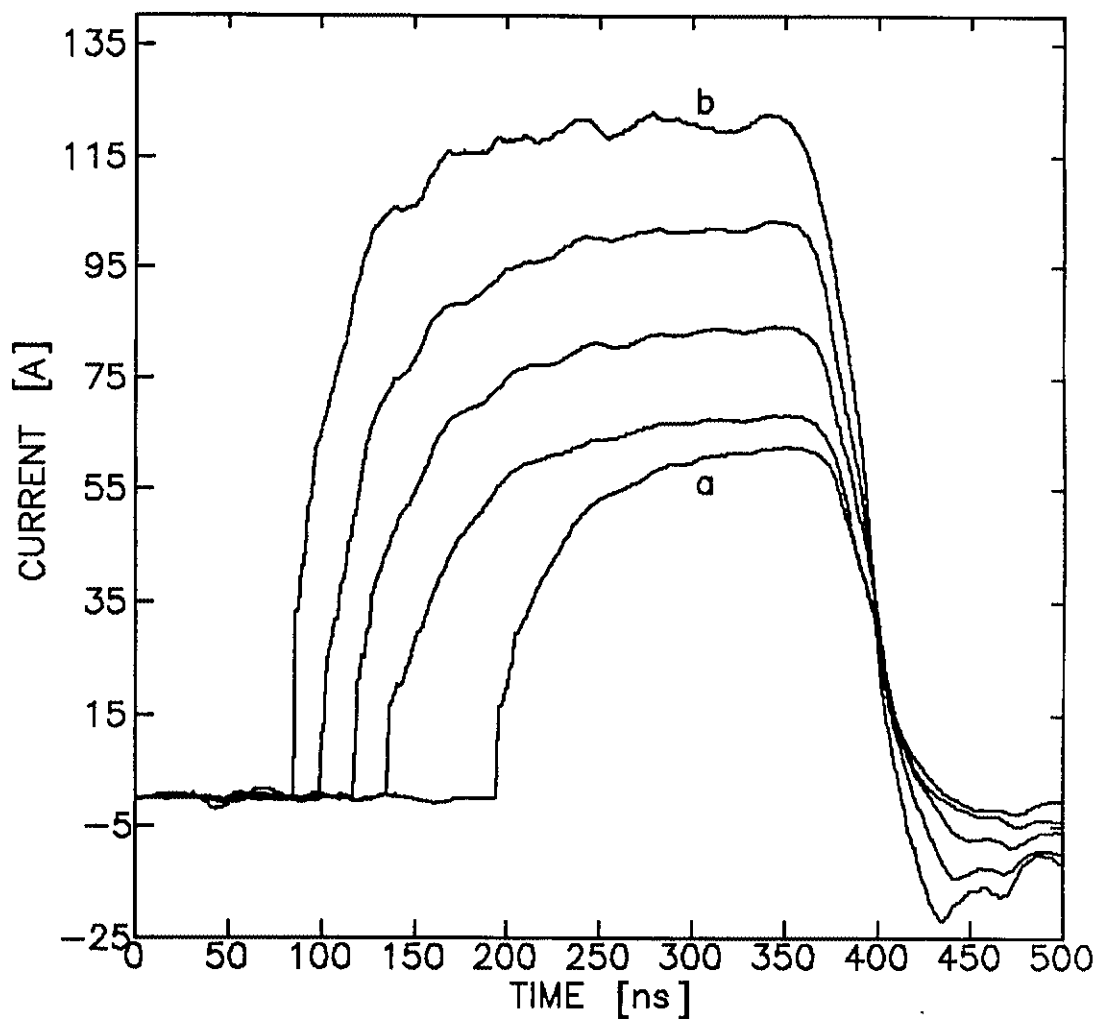


Figure 3-4-3. A series of current waveforms resulting from various applied bias voltages. The bias voltage corresponding to waveform *b* is larger than that for waveform *a*.

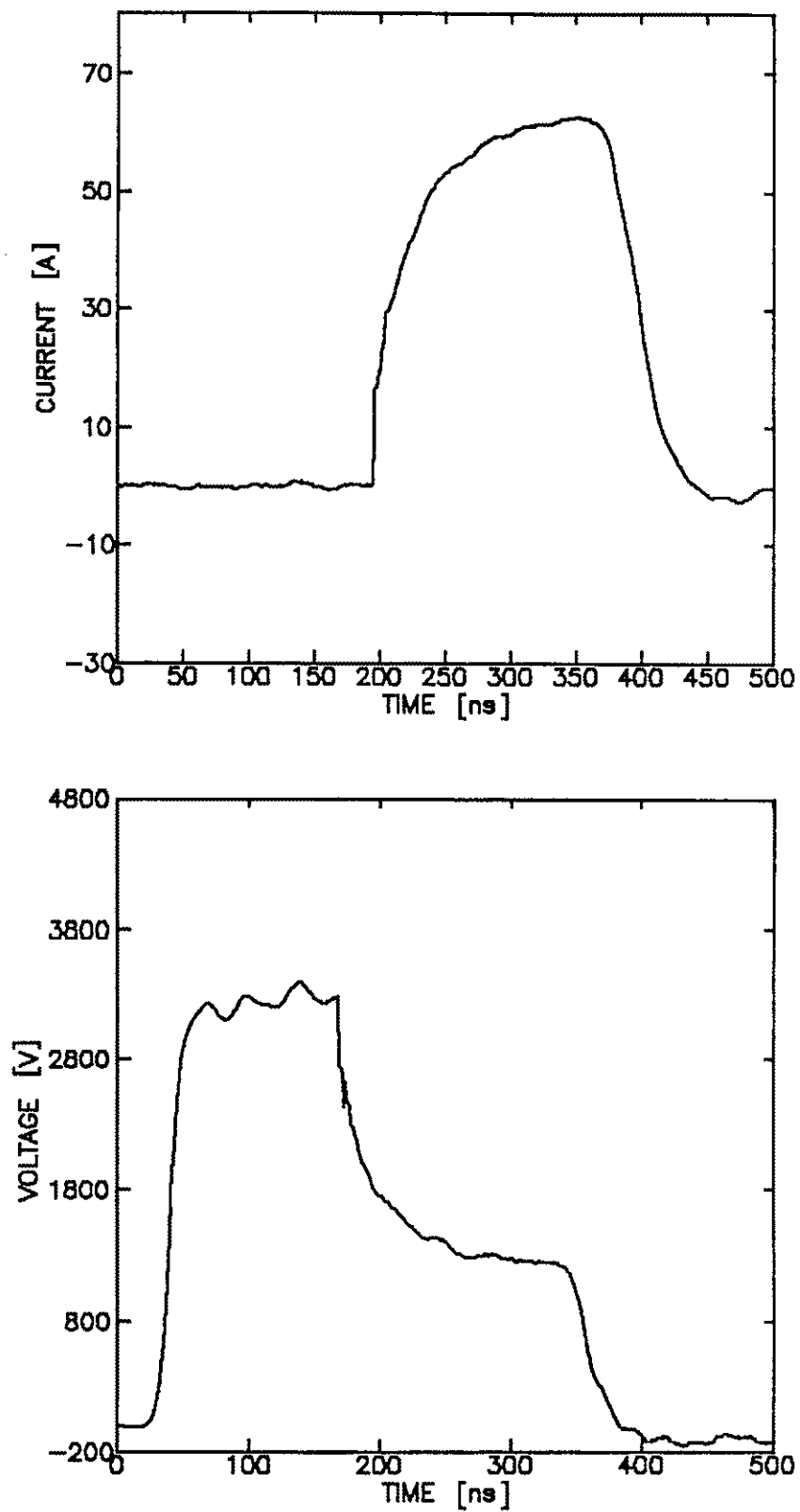


Figure 3-4-4. The current waveform for the curve labeled *a* (top) in figure 3-4-3 with the corresponding applied voltage waveform (bottom).

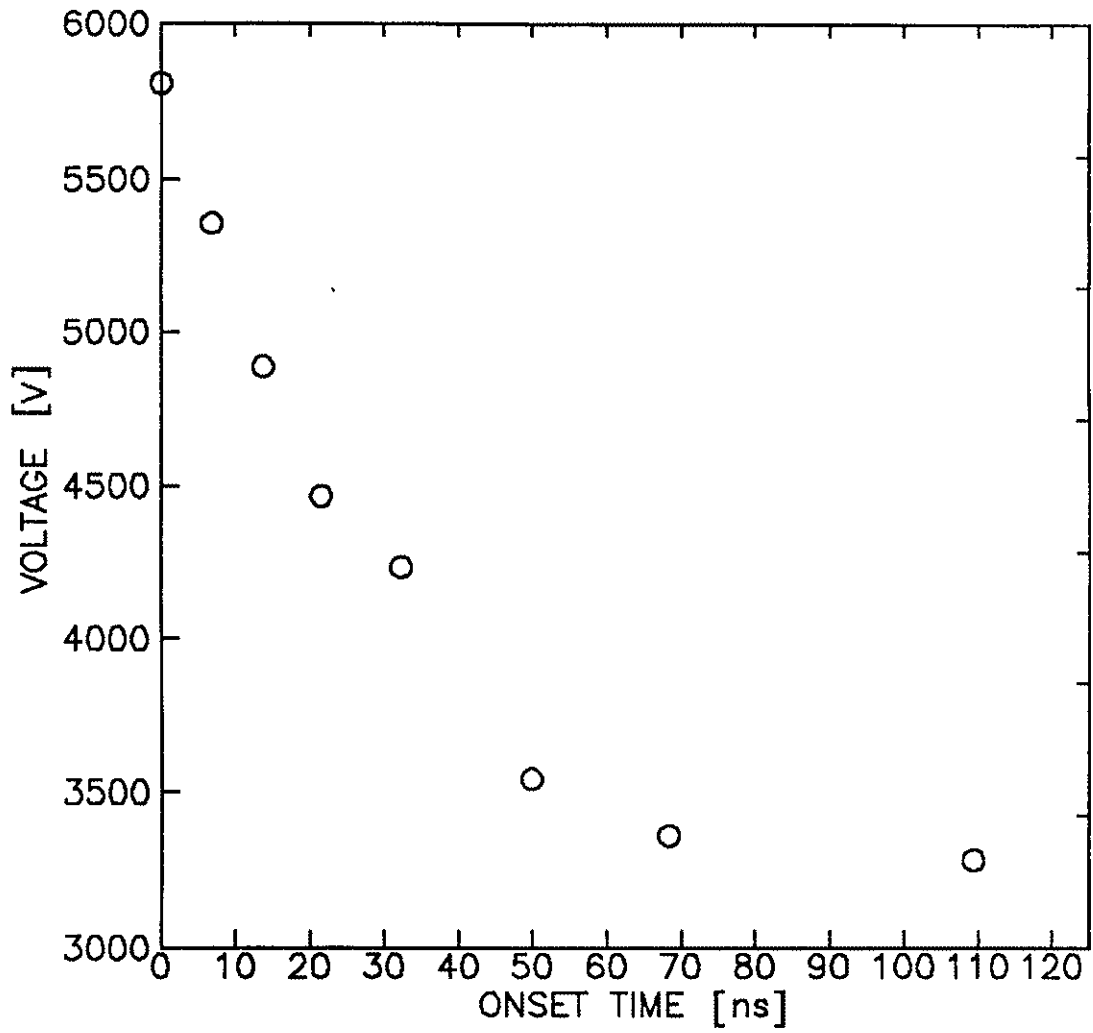


Figure 3-4-5. The dark current onset time vs the applied bias voltage.

observed experimentally as shown in figure 3-4-6. The circuit load line of $30\ \Omega$ imposed on the sample allows the sample voltage and current to be easily obtained through simple circuit theory for currents less than the saturation current. Another interesting observation to be noted is that of the current rate of rise. At applied voltages of 2200 V, the current transition was observed and the current quickly rose to about 16 A in about 5 ns. As the applied voltage was increased, the current rise time decreased to values beyond the bandwidth of the 750 MHz digitizer. At an applied voltage of 6000 V (103 kV/cm), the current rate of rise exceeded 1×10^{11} A/s. The exact rate of rise was not determined because of the bandwidth limitation of the digitizer. Plotting the current after the fast transition against the applied bias before the transition gives the curve shown in figure 3-4-7 (top) whose best fit is linear, crossing the origin with a slope of $150\ \Omega$. Figure 3-4-7 (bottom) shows the current after the fast transition plotted against the voltage just after the transition.

Using the 300 ns pulse from the transmission line pulser, sample 1297-10-A10 (closely compensated) provided similar current and voltage waveforms. A series of current and voltage waveforms were used to generate the I-V curve shown in figure 3-4-8. Negative differential conductivity is again apparent, and the initial rate of rise of the current is similar to that for sample 1297-10-A5. At the lower currents, the I-V relationship does not follow Ohm's law, however, DC I-V measurements show an ohmic behavior at fields of up to 1.4 kV/cm. After the last shot, the sample resistance was measured to be $3\ \text{k}\Omega$, which is much less than the $6\ \text{M}\Omega$ resistance measured before the experiment. The closely compensated samples are very sensitive and are easily damaged. The strongly p-type samples, on the other hand,

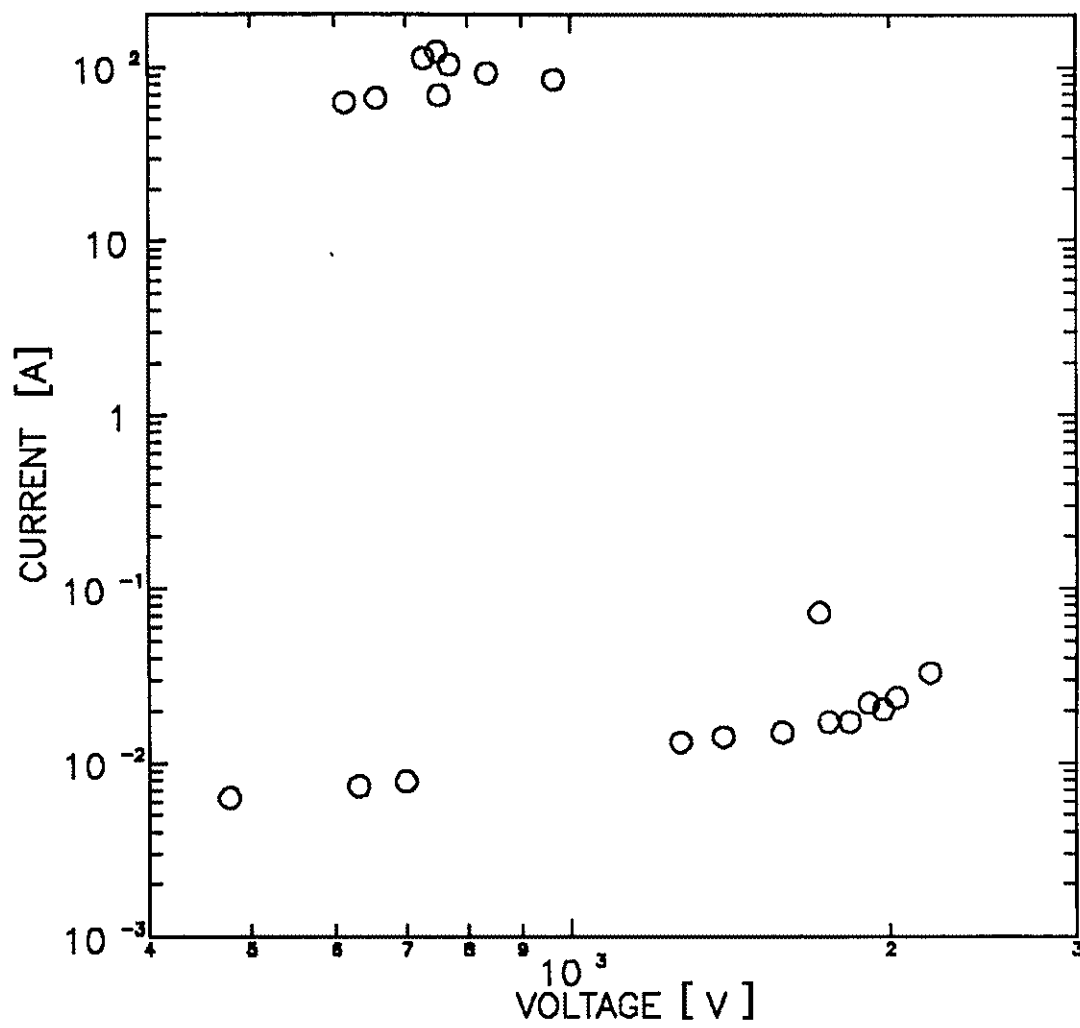


Figure 3-4-6. The I-V curve for sample 1297-10-A5.

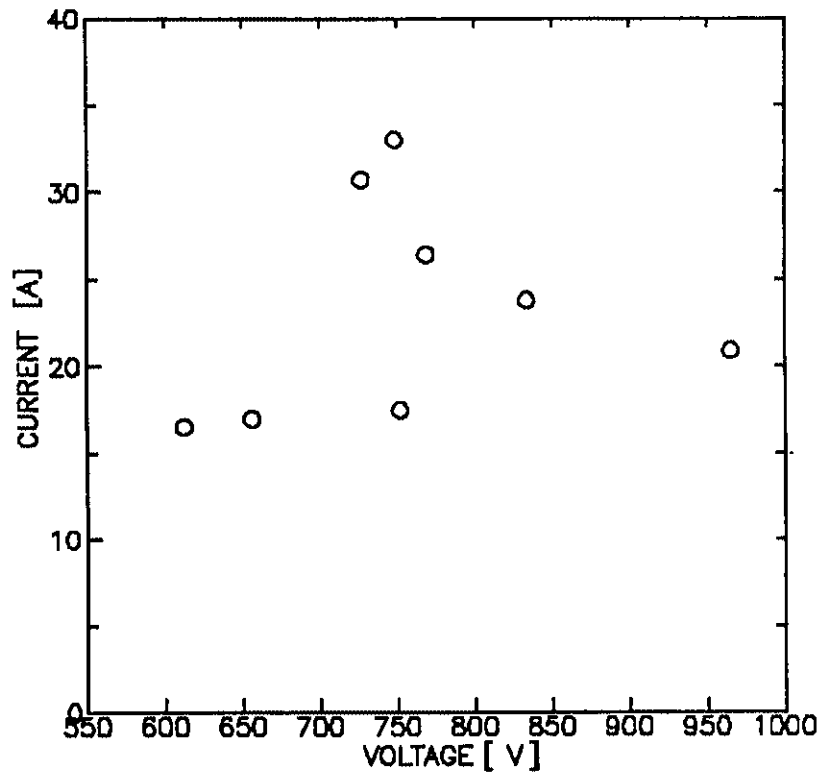
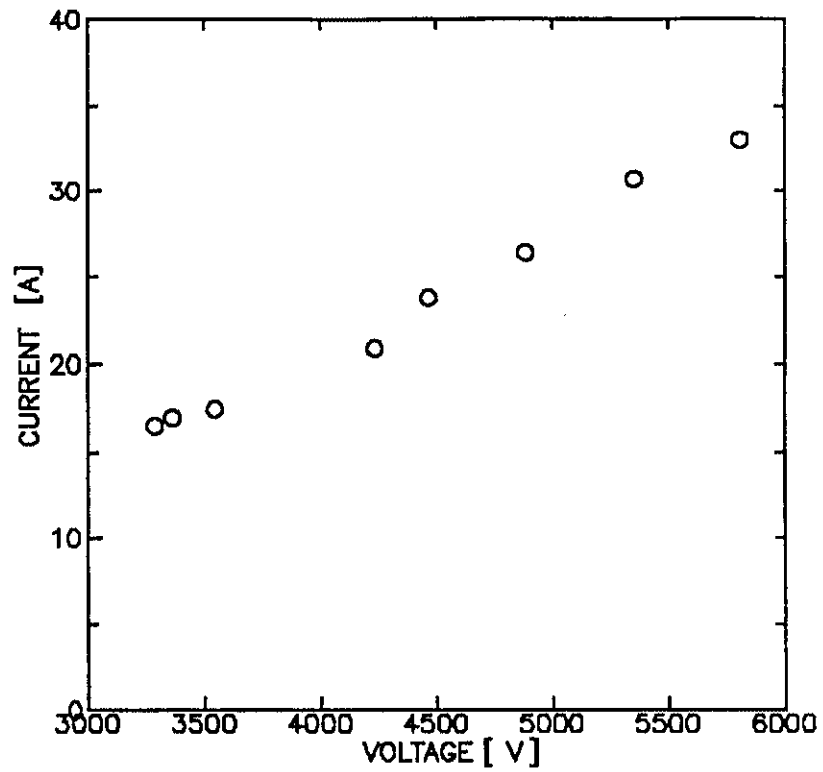


Figure 3-4-7. Current just after the fast transition vs applied bias just before the fast transition (top) and the same current vs the bias voltage just after the fast transition.

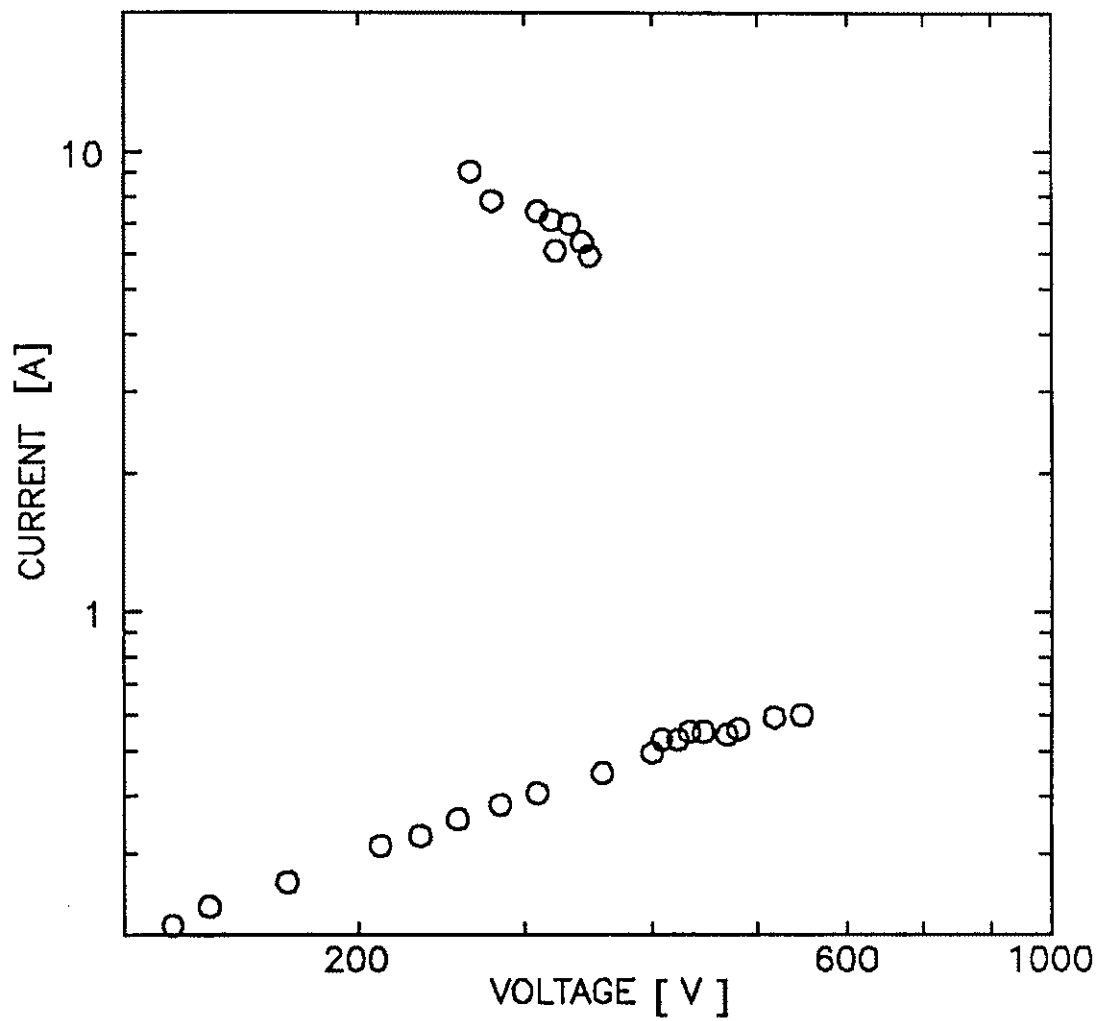


Figure 3-4-8. The I-V curve for sample 1297-10-A10.

seem to be extremely resilient, and they have consistently operated at powers near 1 MW with no apparent damage.

3.5 DISCUSSION

Interest in the I-V characteristics of the switch material is two-fold. First, a basic knowledge of the switch response to high DC, and pulsed voltages is needed. Second, the physical mechanisms controlling the behavior of the switch material can be postulated by investigating the current-voltage characteristics. The two basic effects studied in this chapter were thermal, and trap filling effects. In order to avoid confusion between these effects, the thermal response of the sample was treated both theoretically, and experimentally. It should be noted that thermal emission and crystal heating can be used to explain deviations from Ohm's law only at low currents (mA). After higher currents (greater than a few hundred milli-amperes) are established, double injection and trap filling effects are believed to control the electrical characteristics of the material. This means that the lock-on effect may not be strictly a voltage controlled effect, but thermal emission processes could also be used to trigger lock-on. Therefore, the lock-on currents might be obtained after a thermal run-away of the current. The problem is that the sample will be destroyed during the process if the voltage is applied for too long. If the current is allowed to run away thermally, high currents and a low voltage drop can be established, and the applied voltage can be terminated a short time later by circuit commutation. This will allow for the lock-on currents to be observed and possibly quenched optically,

which would support the idea that these currents are in fact generated by trap filling and double injection.

The next sections focussed on the double injection phenomena. Experiments with strongly p-type GaAs:Si:Cu resulted in electric fields of 32 kV/cm applied across the sample with no temporal development of the dark current (not including thermal effects) during a 40 μ s voltage pulse. Further increase of the field caused a sudden (ns) current increase of three orders of magnitude and a collapse of the voltage across the sample (negative differential conductivity). Experiments with closely compensated (slightly p-type) GaAs:Si:Cu revealed the same ndc, but in this case the voltage collapse occurred at a smaller applied voltage. The theoretical model presented in section 3.3 provided results that matched the experimental trends. Also, the model provides information concerning the *tailoring* of the sample I-V characteristics by processing. The important result is that high currents can be established at a rate exceeding 1×10^{11} A/s by the application of an electric field. With this effect established, the optical quenching of these currents will be discussed in the next chapter.

CHAPTER 4

INFRARED QUENCHING OF LOCK-ON CURRENTS

4.1 THEORY

Chapter 3, and Appendix A involve discussion of the lock-on effect in terms of double injection and the filling of deep traps in the material. This situation is depicted in figure 4-1-1 with a band diagram which shows the deep centers after being filled. One mechanism (steady state dark current) responsible for arriving at the trap filled scenario of figure 4-1-1 has been discussed. The Cu centers are known to be strong hole traps [7], EL2 is an electron trap [33]. The concentrations of these levels are in the range of 10^{16} to 10^{17} cm^{-3} . Through double injection, the centers may be filled with charges leading to the current instabilities described in chapter 3. Also, the lock-on currents can be the same whether they are generated optically or by dark current development. Once the holes are trapped and high currents (amperes) are established, the objective is to optically quench the photocurrent or the dark current.

Obtaining high currents with the dark current is simply accomplished by application of a high electric field for a sufficient amount of time to allow the deep traps to be filled. Once established, the current may be quenched by optically exciting the holes trapped at the copper center into the valence band (see

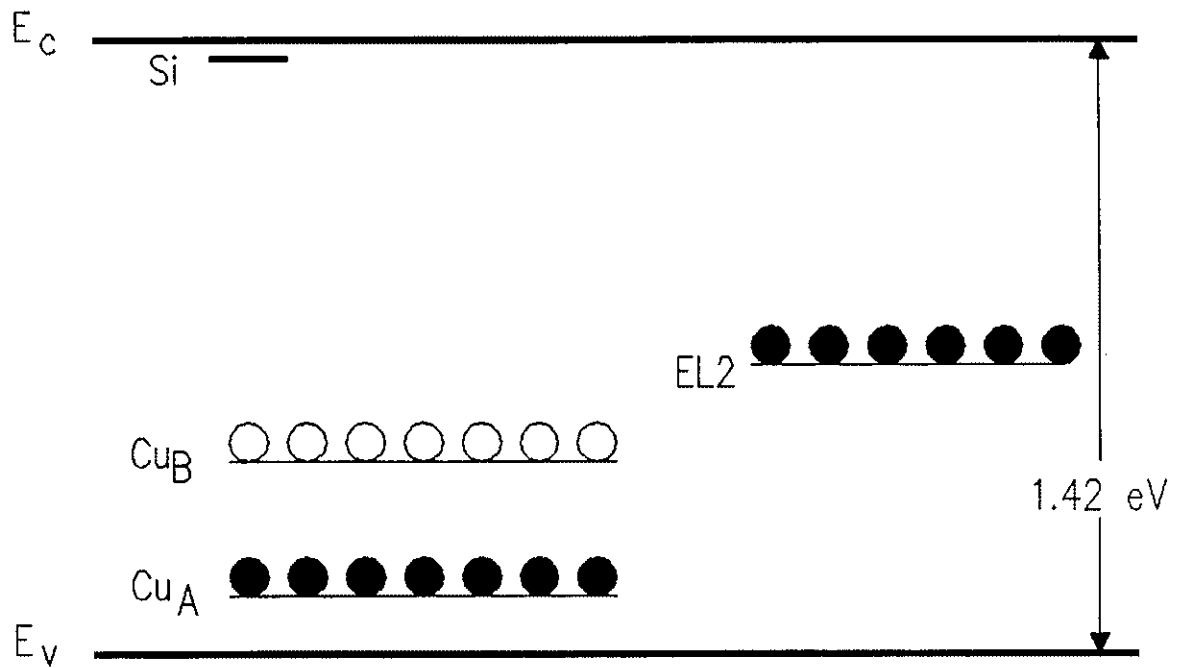


Figure 4-1-1. Band diagram for GaAs:Si:Cu with the traps filled.

figure 4-1-1) giving rise to fast recombination with conduction electrons. The quenching effect can be thought of as a rapid depletion of the free electron density which leads to a smaller conduction current. The lock-on photocurrent generated can be considered to be a superposition of two different phenomena: carriers provided by photo-excitation from Cu_B , and double injection. With high applied bias voltages, the double injection becomes an important consideration in the electrical characteristics. In this case, the Cu_B center is void of electrons and the conduction band has a relatively high density of electrons. The valence band develops a large free hole density after the traps are filled which leads to the current limiting mechanism known as recombination. Infrared quenching via fast recombination may take place by irradiation from a laser pulse sufficient to cause a transition from Cu_B to the valence band while excluding a transition to the conduction band. With a high photon flux, complete quenching of the photocurrent may occur which can cause the temporal development of the subsequent dark current to take some time. In chapter 3, the dark current onset time was found to be field dependent. Now, the onset time may also be dependent on the *quenching factor* which is related to the percent of photocurrent quenched [10,12]. Partial quenching of the photocurrent will only partially empty the copper level giving a small density of excess holes to the valence band, and thus decreasing the time required to re-establish the dark lock-on current. In other words, the higher the quenching factor, the longer it will take for the traps to fill and the current to recover for a given electric field strength. This should be the case whether the current is established optically or by the development of the dark current. The following sections will experimentally support some of these ideas.

4.2 EXPERIMENTS AND RESULTS

The first experiment will involve the quenching of persistent photocurrents. Confusion must be avoided between the persistent photocurrent known as *tail current* which was described in chapter one, and the lock-on persistent photocurrents. For clarity, these two current waveforms are displayed in figure 4-2-1. Note the microsecond decay time in figure 4-2-1 (top) and the extremely long time constant in figure 4-2-1 (bottom). Extremely fast closure times have been reported in other GaAs switches [36]. The purpose of the following experiment will be infrared quenching of currents similar to figure 4-2-1 (bottom).

Experiment

The bias voltage was generated by charging a transmission line through a 1 k Ω resistor as shown in figure 4-2-2. The transmission line used was a 50 Ω , 36 meter long, RG-58 cable (two way transit time = 350 ns). Figure 4-2-2 shows the components of the bias circuit including the method of optical excitation by laser pulses incident on the edge of the sample. In order to ensure impedance matching, the sample was mounted on a 50 Ω microstrip line (same as in chapter 3). The digitizer used (Tektronix 7912AD) was terminated with 50 Ω which also acted as the current viewing resistor.

Optical closing and opening was accomplished using two different laser pulses. The laser used for closing, or more specifically photo-ionization of electrons from the deep copper centers into the conduction band, was a single shot, single wavelength, Nd:YAG solid state laser [34]. This laser is Q-switched and operates at a wavelength

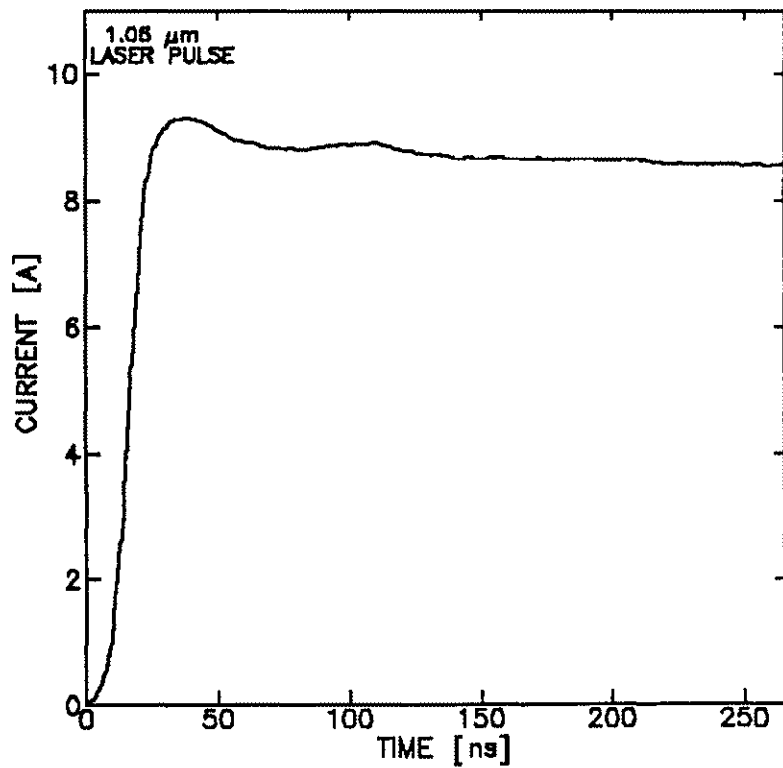
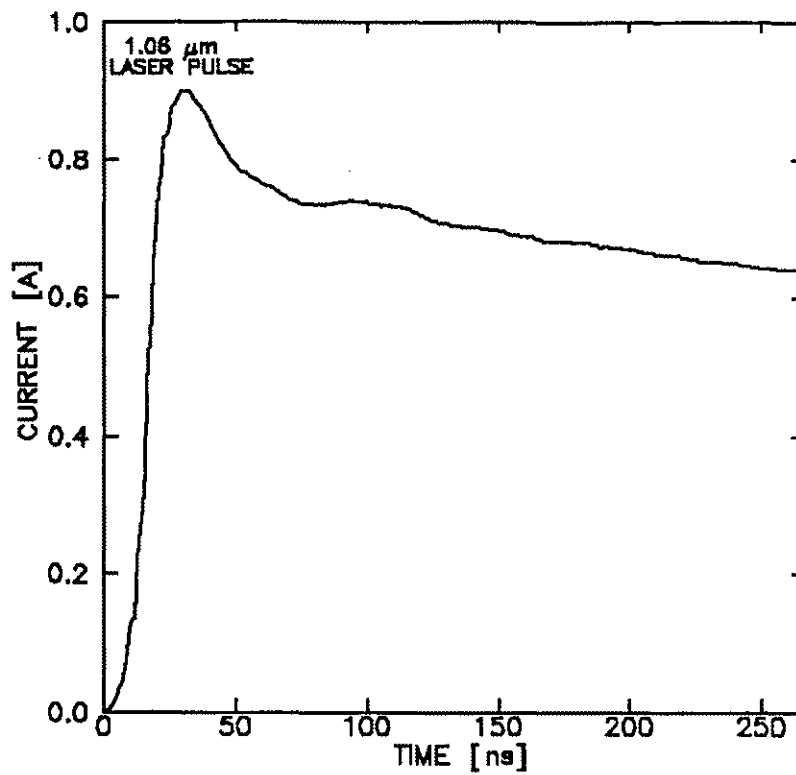


Figure 4-2-1. Photocurrent decay with applied fields below and above the lock-on threshold (top and bottom curves respectively).

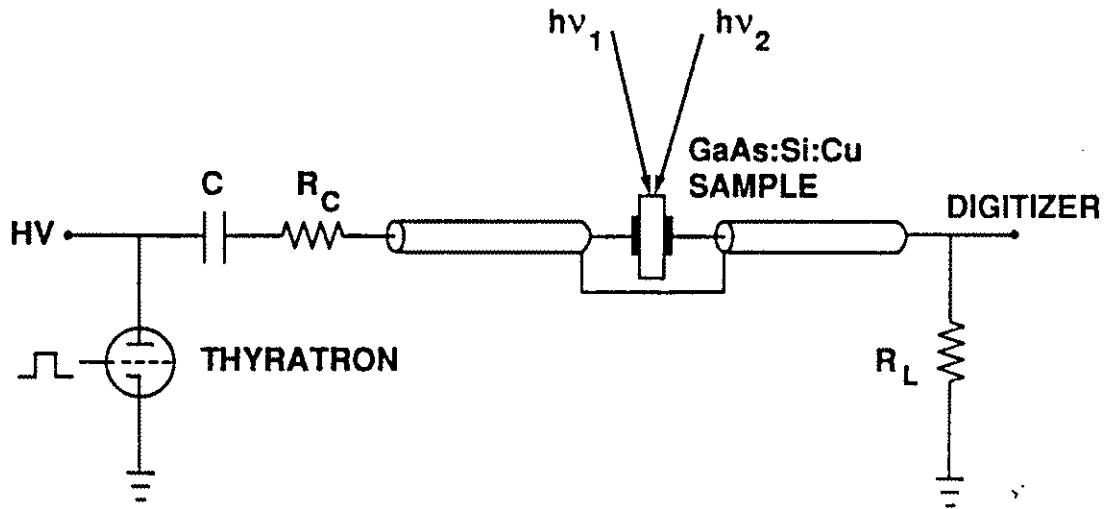


Figure 4-2-2. The bias circuit for use in the photoconductive experiments.

of 1064 nm delivering a nearly Gaussian pulse of 26 ns full width at half maximum (FWHM). This laser is able to deliver approximately 3 mJ.

The laser used for switch opening, or photo-ionization of holes at the copper center into the valence band, was the system manufactured by Spectra Physics (DCR-3). This system uses a frequency doubled Nd:YAG laser pulse to pump a pulsed dye laser (PDL). The PDL output is then mixed with 1064 nm laser light obtaining a sum wavelength of 1700 nm. The output pulse is roughly Gaussian with a FWHM of 7 ns. The output 1700 nm laser pulse had an energy of approximately 0.5 mJ.

Results

The photocurrent measurements were performed for different bias voltages. At low electric fields (less than 3 kV/cm), the photo-induced current decays over a time of microseconds due to the relatively slow capture of electrons at the Cu_B center (figure 4-2-1 (top)). The sample used to obtain the current waveform of figure 4-2-1 (top) was pulse charged to a voltage of 50 V corresponding to an average electric field of 0.8 kV/cm. At electric fields greater than 3 kV/cm, the switch is characterized by photocurrents which do not change over the time scale shown in figure 4-2-1 (bottom). Plotting the current-voltage characteristics at a time of 250 ns for fields across the sample starting at less than 1 kV/cm and continuing through 21 kV/cm gives the results shown in figure 4-2-3. At lower fields the sample behaves in an ohmic manner corresponding to a switch resistance of approximately 70 Ω . At about 200 V, a break point is observed where the current transitions to a super-linear

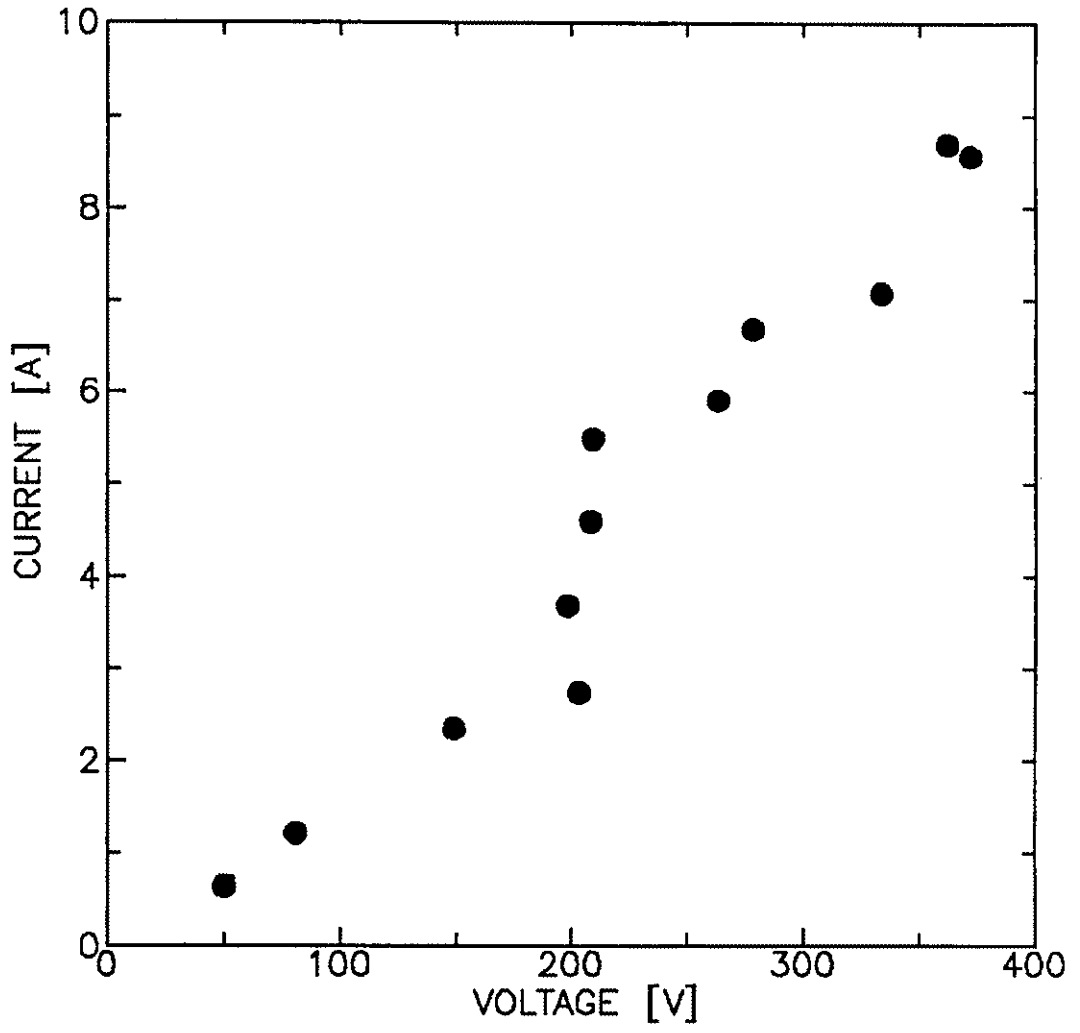


Figure 4-2-3. The I-V curve for the photocurrent data (see figure 4-2-1) [19,38].

dependence. This break point is considered to be the transition of the sample into what is known as the lock-on effect.

Quenching of the persistent photocurrent using infrared radiation was accomplished and is shown in figure 4-2-4 [19]. Possibly due to low laser intensity, complete quenching was not accomplished. After quenching of the photocurrent (figure 4-2-4) and a delay of 25 ns, the current rapidly transitions to a steady value without further illumination. This value is less than the photocurrent previously established. A comparison with the quenching effect at fields less than 3 kV/cm shows that the photocurrent was quenched to the same degree as for fields greater than 3 kV/cm (figure 4-2-5). However, the current after quenching stayed at a value determined by the laser intensity. With sufficient laser power, complete quenching of the photocurrent was demonstrated [5]. The contact geometry used for figure 4-2-5 was planar which involved a larger gap space, higher voltage, and higher current at the same field strength as with the sandwich contacts.

4.3 DISCUSSION

A sharp rise of the current-voltage characteristic over a 2.5 A to 5.5 A range of current for a change of voltage of a few volts was observed in the photoconductive experiments. Figure 4-3-1 shows a hypothetical dark I-V curve (solid line), created based on the results of chapter 3, plotted together with the experimental photoconductivity I-V data (circles). The temporal behavior seen in figure 4-2-1 can be understood by considering the various steady state currents at different applied voltages. Point P_1 in figure 4-3-1 represents the photocurrent obtained after optical

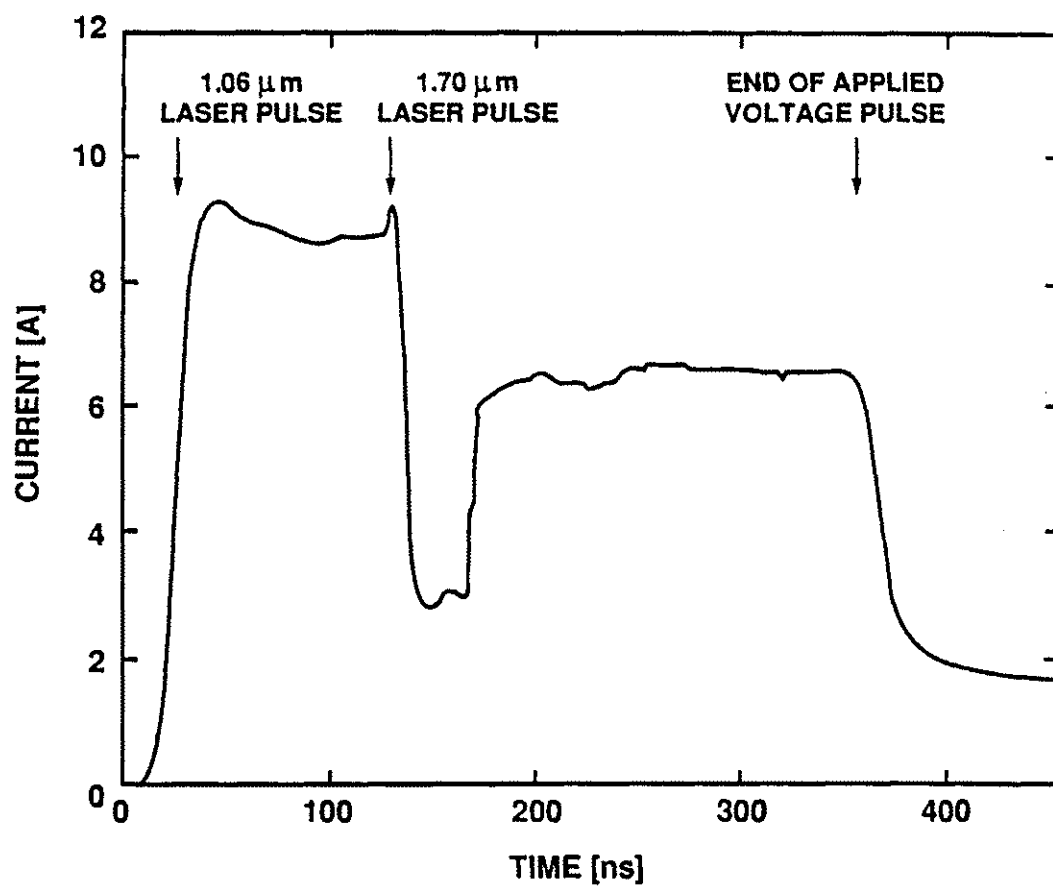


Figure 4-2-4. Infrared quenching of lock-on photocurrent.

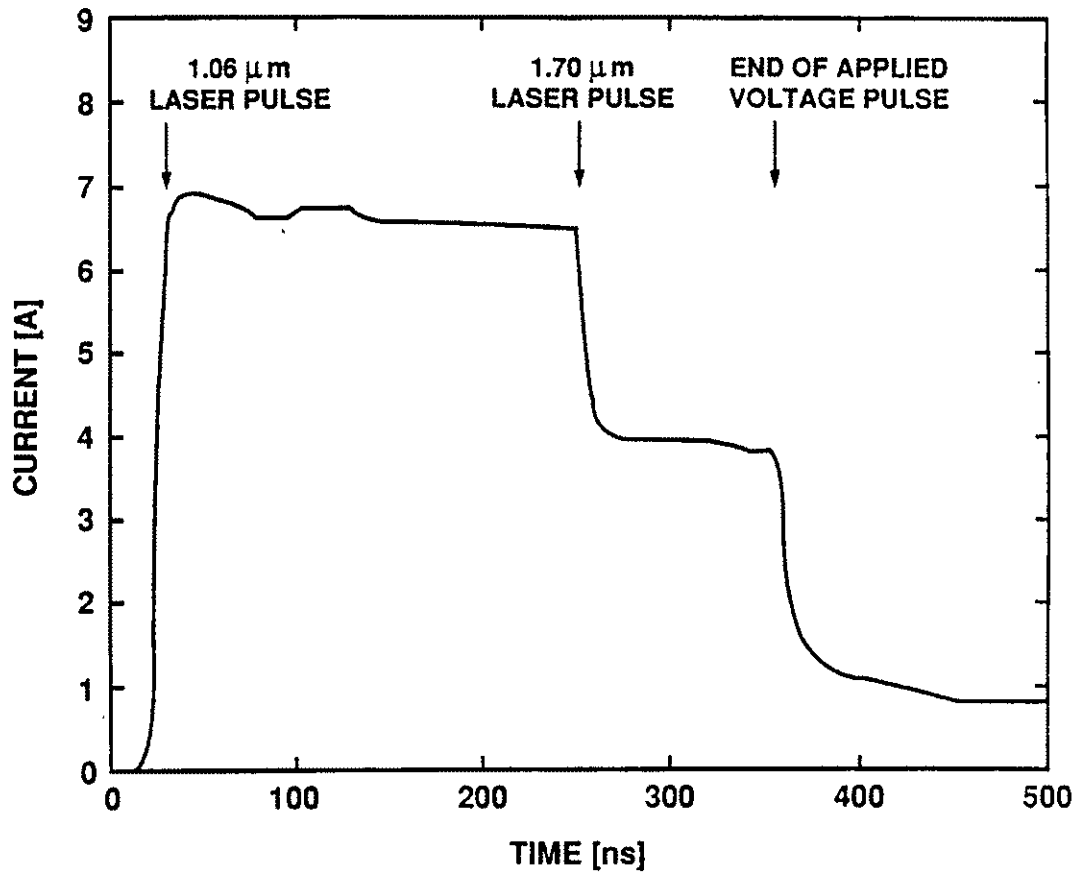


Figure 4-2-5. Infrared quenching of photocurrent below the lock-on threshold.

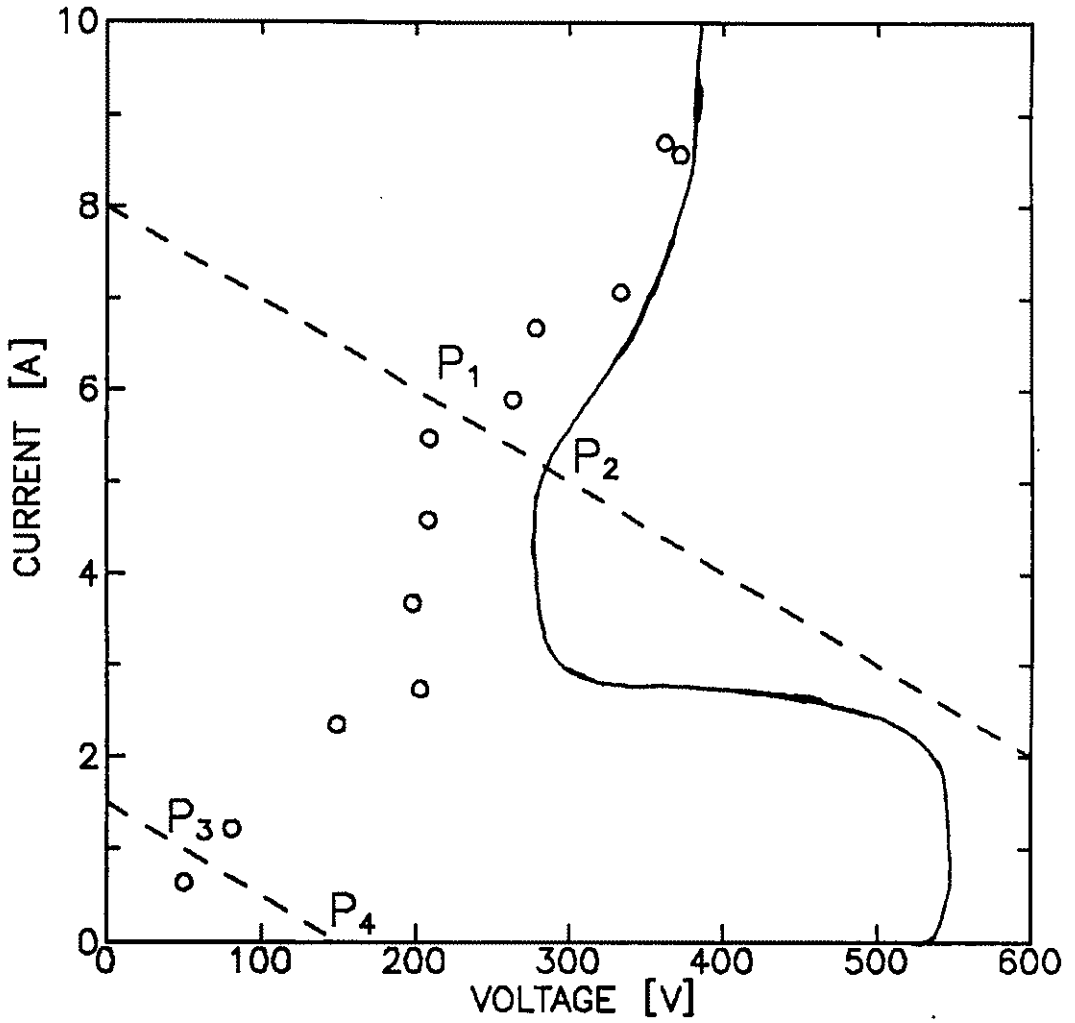


Figure 4-3-1. A hypothetical dark current curve (solid line) plotted together with the experimental I-V data from figure 4-2-3. The imposed load lines are shown with dashed lined.

excitation (similar to figure 4-2-4). After infrared quenching of this photocurrent, a delay of 25 ns is observed with the bias still applied, followed by a rapid dark current development to the point labeled P_2 , which is less than the photocurrent value. Based on the results of section 3.3, this current recovery level may be a steady state value. Consider the load line scenario of figure 4-3-1 where the load line (upper, dashed line) intersects the dark I-V curve at one point. The load line can also be imposed such that it intersects the dark current curve in three different places, which is an unstable situation and results in the formation of filaments. As a result, the dark current may develop to a steady state value that is less than the photocurrent. For complete quenching of the photocurrent and no subsequent dark current development, the switch must be operated at voltages where the load line intersects the zero current line for the ideal dark current curve (P_3 and P_4).

CHAPTER 5

CONCLUSIONS

5.1 DISCUSSION OF RESULTS

Absorption of Radiation in GaAs

The absorption depth for GaAs with various doping profiles was measured. The absorption depth of 1.064 μm laser radiation was found to be approximately 3 mm in GaAs:Si:Cu. Silicon doped, and semi-insulating GaAs were shown to have 8 mm absorption depths. This determines the possible contact geometries that may be used for high voltage applications. The absorption results also provide a calibration for the use of wavelengths longer than 1.064 μm , which will have a smaller absorption coefficient.

Also of importance is the effect of the copper density on the absorption characteristics. The sample used in the experiment had a silicon density of $4.7 \times 10^{16} \text{ cm}^{-3}$. The copper introduced into the host crystal was doped such that the sample was strongly p-type (Cu density $> 1 \times 10^{17} \text{ cm}^{-3}$). Copper doping caused a factor of three shift in the absorption depth. The relative densities of copper and silicon in the material determine the number of electrons trapped at the copper level which, in turn, effects the absorption characteristics. The densities of copper and

silicon may be adjusted to provide optimum absorption properties (ie. longer absorption lengths), while maintaining sufficient electrical response with respect to high on-state current conduction. The $1/e$ absorption length for semi-insulating GaAs was found to be 8 mm. This result provides information concerning the limit to which the absorption depth may be shifted by the controlled doping of silicon and copper.

Thermal Effects

Thermal effects were explored to obtain information concerning the steady state thermal stability of the switch. A thermal model was presented with results from experiments conducted to characterize the heat equation which describes the overheating in the crystal. The value for the heat loss to the environment (air) was found to be 3.03 W/kg·K. For example, the thermal response of the crystal to high repetition pulses may be determined. The experiments have shown that the current becomes unstable at average power dissipation levels of a few hundred milli-watts. A larger value for the heat loss to the environment can be obtained by improving the thermal environment of the sample (using oil, for example), and therefore allowing the switch to be operated at higher powers.

The thermal analysis verified that a deviation from Ohm's law due to thermal processes does not constitute a current instability until a threshold power dissipation level is reached, and this was observed experimentally. Also, at sufficiently high electric fields, current instabilities due to thermal effects, and not due to trap filling effects, were observed. The purpose of the thermal analysis is to distinguish between

the vertical current transition due to trap filling effects observed in semi-insulating GaAs [5,24], and thermal instabilities. For GaAs:Cu:Si, thermal instabilities were observed at fields of 2.3 kV/cm in air, and 3.4 kV/cm in room temperature transformer oil.

Dark Current

The dark current was measured by applying fast (300 - 600 ns) voltage pulses, and measuring the voltage across a resistor that is in series with the sample. A temporal development of the dark current was found to occur at electric fields of greater than 31 kV/cm. The current development rate exceeded 1×10^{11} A/s with electric fields above 90 kV/cm. This rapid current development is probably the result of impact ionization of deep impurity levels due to high local electric fields, which may be accompanied by the formation of filaments. This effect can be used as the turn-on mechanism for a closing switch, or as a method to *sharpen* electrical pulses which have relatively slow risetimes. Similar pulse sharpening techniques have been used with silicon to develop pulses with 30 ps risetimes [37]. The peak voltage and current obtained with the dark current development corresponds to operation near 1 MW, single shot.

Plotting the I-V data (after the current development - if any) provided curves that displayed negative differential conductivity. The measured results provide a good qualitative agreement with the theoretical model which also shows negative differential conductivity for a semiconductor with multiple deep traps. The model, however, shows a poor quantitative agreement with experiment because the model

is based on a system with three energy levels in the bandgap, which is probably an over-simplification of the complicated deep level structure of doped GaAs. The maximum voltage hold-off can be experimentally found by varying the load line of the pulse forming circuit. This will allow the negative differential conductivity results to be mapped out more clearly in the form of I-V curves. An example of this method is outlined in figure 5-1-1.

Quenching of Lock-On Currents

The lock-on currents have been shown to be either the result of optical excitation with sufficient electric fields applied, or by the temporal development of the dark current and negative differential conductivity. Quenching of the lock-on photocurrent was shown, and the subsequent development of the dark current was observed. The time delay between the quenching and the dark current development is assumed to be adjustable based on the degree to which the photocurrent was quenched (for a given bias voltage). The measured time delay before the recovery of the current after quenching was 25 ns for a laser energy of 0.3 mJ [19,38]. The time delay for dark current recovery after complete quenching of the photocurrent may be varied by changing the applied bias voltage according to figure 3-4-5 (dark current onset time vs applied bias voltage). For an applied bias voltage of 5.4 kV, the dark current onset time was found to be 10 ns which is very short compared to the 110 ns onset time for an applied voltage of 3.3 kV. Applied voltages greater than 5.8 kV (100 kV/cm) caused the dark current onset time to appear to be instantaneous on the time scale of the experiment.

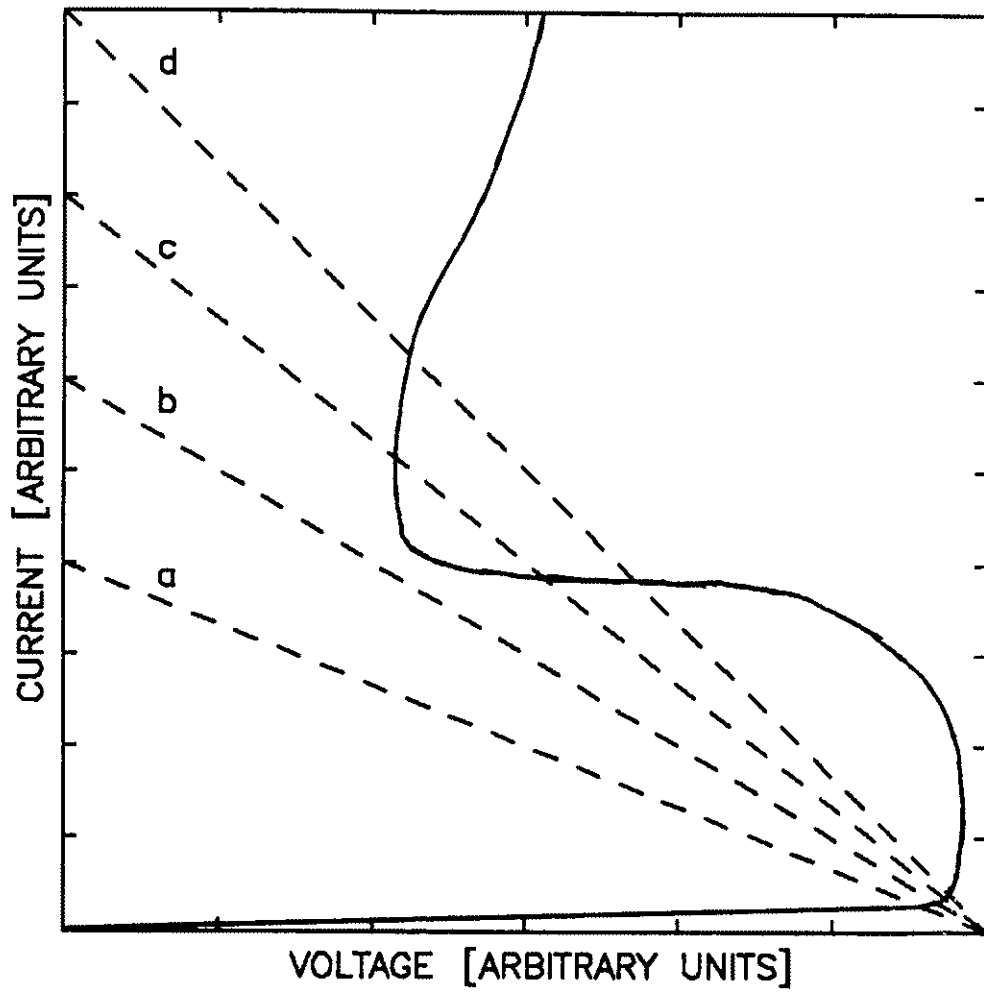


Figure 5-2-1. An I-V curve showing the negative differential conductivity with various load lines for a fixed bias voltage.

Since the photo, and dark lock-on currents are assumed to be the same, it seems reasonable to use the same concept (BOSS) for the quenching of either of these currents. Once the load line corresponding to the maximum hold-off voltage is found corresponding to the smallest current, the sample could then be biased in such a way that the load line intersects the dark I-V curve at a maximum voltage and low current point, but passes very near to the low voltage - high current part of the I-V curve (load-line *b* in figure 5-1-1). The sample may then be *kicked* into lock-on by the application of a very low intensity laser pulse provided that the I-V curve under illumination is similar to, or the same as, the dark I-V curve. At the high *on-state* conduction currents, this is a valid assumption based on the results described previously where the photo and dark I-V curves were found to coincide at high currents. A transient simulation of the dark current has shown that this process may take a few hundred picoseconds for a source function of $10^{25}\text{cm}^{-3}\text{s}^{-1}$, and an estimation based on a trap density of 10^{16}cm^{-3} and a source function of $10^{17}\text{cm}^{-3}\text{s}^{-1}$ leads to a time delay of 100 ms [39]. This time delay is due to the trap filling time of the deep levels. The quenching of the resulting photocurrent should follow the same behavior as the quenching of lock-on photocurrents. The temporal development of the dark current may be used as the turn-on mechanism instead of providing photocarriers with a laser pulse, and the resulting lock-on current may then be quenched by the same method as shown for photocurrent quenching. This would allow a switch to be operated in repetition without using a laser pulse to repetitively initiate the load current.

5.2 FUTURE WORK

The results of this work have created many other avenues for the direction of future research in the field of bulk GaAs switches. The first, and probably most important, is the material processing. The diffusion system used to create compensated samples in this and other work [11,12,35], must be improved. Material processing must be controlled with respect to the contents of the diffusion environment, and contact application. The presence of different, and usually uncontrollable, impurities in the diffusion environment gives rise to various energy levels in the bandgap. The arsenic content of the diffusion environment, for example, plays a very important role in the successful, consistent compensation of silicon doped GaAs. Air, which is also present, raises the question of the effect of oxygen doping. Diffusion, and electrical compensation in GaAs may be further studied in [40-44], and [11,45-48] respectively. Completely controlled diffusion of copper into GaAs must be placed high on the priority list in order to develop a practical switch.

The research contained in this document can be further extended by studying effects such as the absorption of radiation at different wavelengths. Specifically, the absorption of radiation used for optical quenching ($1.7 \mu\text{m}$) should be determined. The absorption characteristics during high current conduction may also be desired. The switch scaling could then be determined for a device designed to operate without the optical excitation from the $1 \mu\text{m}$ laser pulse (ie. dark current quenching).

5.3 FINAL REMARKS

The effort involved in producing this document was, without question, worth every minute, because of the opportunity to be involved in such an exciting field. I must emphasize that the research concerning bulk GaAs switching will require much more persistence in resolving the topics that have been discussed here and in previous work [5,11,12,35]. A great deal of positive results have been generated in the past two years and the progress of the project is evidence of that. The research to be carried out in the next few years will determine the short term success or failure of the concept and the implementation. For this reason, I believe that the exciting time to be involved in this research is just beginning.

LIST OF REFERENCES

- [1] J.H. Hur, P. Hadizad, S.R. Hummel, P.D. Dapkus, H.R. Fetterman, M.A. Gundersen, "GaAs Opto-Thyristor for Pulsed Power Applications," Proceedings of the 19th Power Modulator Symposium, San Diego California, 1990.
- [2] G.M. Loubriel, M.W. O'Malley, and F.J. Zutavern, "Toward Pulsed Power Uses for Photoconductive Semiconductor Switches," in the Proc. of 6th IEEE Pulsed Power Conference, P.J. Turchi and B.H. Bernstein, Eds., New York: IEEE, 1987, pp. 145-148.
- [3] F.J. Zutavern, G.M. Loubriel, and M.W. O'malley, "Recent Developments in Opening Photoconductive Semiconductor Switches," Proceedings of the 6th IEEE Pulsed Power Conference, P.J. Turchi and B.H. Bernstein, Eds. New York: IEEE, 1987, pp. 577-580.
- [4] S.M. Sze, Semiconductor Devices: Physics and Technology, John Wiley and Sons: New York, 1985.
- [5] D. Stoudt, "Electrical Characteristics of Semi-Insulating GaAs: A Material For High Power Switches," Master's Thesis, Dept. of Electrical Engineering, Old Dominion University, Norfolk, Virginia, 1989.
- [6] D.C. Stoudt, K.H. Schoenbach, V.K. Lakdawala, "The Electrical Characteristics of Semi-Insulating GaAs for High Power Switches," presented at the Seventh IEEE Pulsed Power Conference, Monterey, CA, June 11-14, 1989, pp. 348-351.
- [7] K.H. Schoenbach, V.K. Lakdawala, R. Germer, and S.T. Ko, "An Optically Controlled Closing and Opening Semiconductor Switch," *J. Appl. Phys.*, **63** (7), 2460-2463, 1988.
- [8] M.S. Mazzola, K.H. Schoenbach, V.K. Lakdawala, and R. Germer, "GaAs Photoconductive Closing Switches With High Dark Resistance and Microsecond Conductivity Decay," *Appl. Phys. Lett.* **54** (8), 742-744, 1989.

- [9] M.S. Mazzola, K.H. Schoenbach, V.K. Lakdawala, and S.T. Ko, "Investigation of a Photoconductive Closing and Opening Bulk GaAs Semiconductor Switch," presented at the Seventh IEEE Pulsed Power Conference, Monterey, California, June 11-14, 1989, pp. 418-421.
- [10] M.S. Mazzola, K.H. Schoenbach, V.K. Lakdawala, and S.T. Ko, "Nanosecond Optical Quenching of Photoconductivity in a Bulk GaAs Switch," *Appl. Phys. Lett.* **55** (20), 2102-2104, 1989.
- [11] M.S. Mazzola, "Experimental Studies of Bulk Optically Controlled GaAs Switches Utilizing Fast Infrared Quenching," Ph.D. Dissertation, Dept. of Electrical and Computer Engineering, Old Dominion University, Norfolk, Virginia, 1990.
- [12] S.T. Ko, "Study of Direct Semiconductor Materials for an Optically Controlled Switch," Ph. D Dissertation, Department of Electrical and Computer Engineering, Old Dominion University, Norfolk, Virginia, 1989.
- [13] H.J. Queisser and D.E. Theodorou, "Hall-Effect Analysis of Persistent Photocurrents in n-GaAs Layers," *Phys. Rev. Lett.*, **43**(5), 401-404, 1979.
- [14] J.I. Pankove, "Absorption Edge of Impure Gallium Arsenide," *Phys Rev.* **140**, A2059, 1965
- [15] J.I. Pankove, Optical Processes in Semiconductors, Dover Publications: New York, 1971 pp. 47, 103.
- [16] Michael G. Clark, "Calculation of Carrier Equilibrium Effects in Transition-Metal Doped Semiconductors with Application to Cr-Doped GaAs," *J. Phys. C:Solid St. Phys.*, **13**, 2311, 1980.
- [17] S.M. Sze, Physics of Semiconductor Devices, John Wiley and Sons, Inc.: New York, 1969.
- [18] R.A. Smith, Semiconductors, Cambridge University Press: New York, 1978, pp. 291-342.
- [19] R.A. Roush, M.S. Mazzola, K.H. Schoenbach, V.K. Lakdawala, "Optical Quenching of Lock-On Currents in GaAs:Si:Cu Switches," Proceedings of the 19th IEEE Power Modulator Conference, San Diego, California, 1990.
- [20] E.G.S. Paige and G.D. Rees, "Absorption Edge of GaAs and It's Dependence on Electric Field," *Phys. Rev Lett.*, **16**, 444, 1966.

- [21] D.Redfield, M.A. Afromowitz, "The Direct Absorption Edge in Covalent Solids," *Appl. Phys. Lett.*, 11, 138, 1967.
- [22] Ralf Peter Brinkmann, private communication.
- [23] J.S. Blakemore, "Semiconducting and Other Major Properties of Gallium Arsenide," *J. Appl. Phys.*, 53(10), R123, 1982.
- [24] Murray A. Lampert, and Peter Mark, Current Injection in Solids, Academic Press: New York, 1970, pp. 15-40, 140-154, 207-215, 277-324.
- [25] R. Baron and J.W. Mayer, "Double Injection in Semiconductors," in Semiconductors and Semimetals - Injection Phenomena, Volume 6, R.K. Willardson and A.C. Beer, Eds., Academic Press, Inc.: New York, 1970, pp. 141-195, 202-282.
- [26] N. Holonyak, Jr., "Double Injection Diodes and Related DI Phenomena in Semiconductors," *Proc. IRE*, 50, 2421, 1962.
- [27] Esther M. Conwell, High Field Transport in Semiconductors, Academic Press: New York, 1967, pp. 80-99.
- [28] Juras Pozhela, Plasma and Current Instabilities in Semiconductors, Pergamon Press: New York, 1981, pp. 241-242.
- [29] A.M. Barnett, "Current Filament Formation," in Semiconductors and Semimetals - Injection Phenomena, Vol. 6, R.K. Willardson and A.C. Beer, Eds., Academic Press, Inc.: New York, 1970, pp. 141-200.
- [30] A.M. Barnett, and H.A. Jensen, "Observation of Current Filaments in Semi-Insulating GaAs," *Appl. Phys. Lett.*, 12, 341, 1968.
- [31] R.P. Brinkmann, "Modeling of Electron-Beam-Controlled Semiconductor Switches," *J. Appl. Phys.*, 68, 318-323, 1990.
- [32] R. P. Brinkmann, K.H. Schoenbach, V.K. Lakdawala, and Mike Kennedy, "The Lock-On Effect in Electron-Beam Controlled GaAs Switches," Proceedings of the 1990 19th Power Modulator Symposium, San Diego California.
- [33] D.V. Lang, and R.A. Logan, "A Study of Deep Levels in GaAs By Capacitance Spectroscopy," *J. Elect. Mat.*, 4(5), 1053-1066, 1975.
- [34] Mini-YAG laser was designed and constructed by Mike Mazzola, currently with Naval Surface Warfare Center, Dahlgren, Virginia.

- [35] G. Baravedia, "Deep Level Characterization in GaAs," Master's Thesis, Dept. of Electrical and Computer Engineering, Old Dominion University, 1990.
- [36] C.H.Lee, Picosecond Optoelectronic Devices, Academic Press: Orlando, FL, 1984.
- [37] M.D. Pocha, J.D. Morse, C.F. McConaghy, C.G. Dease, "Of Kilovolts and Picoseconds: Photoconductive Semiconductors for Diagnostics and Pulse Forming," in *Energy and Technology Review*, Lawrence Livermore National Laboratory, April, 1987, pp. 28-40.
- [38] M.S. Mazzola, K.H. Schoenbach, V.K. Lakdawala, and R.A. Roush, "Infrared Quenching of Conductivity at High Electric Fields in a Bulk, Copper-Compensated Optically Activated GaAs Switch," *IEEE Transactions on Electron Devices*, 37(12), 1990.
- [39] R.P. Brinkmann, K.H. Schoenbach, R.A. Roush, D.C. Stoudt, V.K. Lakdawala, and G.A. Gerdin, "High Power Switching With Electron-Beam Controlled Semiconductors," *Proceedings of the IEEE SPIE Conference*, Boston, Mass., 1990.
- [40] B.I. Boltaks, Diffusion in Semiconductors, Academic Press: New York, NY, 1963.
- [41] Brian Tuck, Atomic Diffusion in III-V Semiconductors, IOP Publishing Ltd., Bristol, England, 1988.
- [42] N. Kullendorff, L. Jansson, and L-A Ledebø, "Copper-Related Deep Level Defects in III-V semiconductors," *J. Appl. Phys.*, 32, 3203-3212, 1983.
- [43] R.N. Hall and J.H. Racette, "Diffusion and Solubility of Copper in Extrinsic and Intrinsic Germanium, Silicon, and Gallium Arsenide," *J. Appl. Phys.*, 35, 379-397, 1964.
- [44] P.W. Hutchinson and R.K. Ball, "A Study of the Effects of Annealing, Zinc Diffusion, and Copper Diffusion on the Defect Structure of Silicon-Doped GaAs," *J. Mat. Sci.*, 17, 406-416, 1982.
- [45] E.J. Johnson, J.A. Kafalas, and R.W. Davies, "The Role of Deep-Level Centers and Compensation in Producing SI GaAs," *J. Appl. Phys.*, 54(1), 204-207, 1983.
- [46] J. Blanc, R.H. Bube, and H.E. MacDonald, "Properties of High-Resistivity Gallium Arsenide Compensated with Diffused Copper," *J. Appl. Phys.*, 32, 1666-1679, 1961.

- [47] G. M. Martin, J.P. Farges, G. Jacob, J.P. Hallais, and G. Poiblaud, "Compensation Mechanisms in GaAs," J. Appl. Phys., 51, 2840-2852, 1980.
- [48] R. Zucca, "Electrical Compensation in Semi-Insulating GaAs," J.Appl. Phys., 48,1987-1994, 1977.
- [49] This information was obtained using a model of the steady state I-V characteristics for GaAs with multiple deep traps developed by R.P. Brinkmann, Old Dominion University, Physical Electronics Research Institute, Norfolk, Virginia.

APPENDIX A

THE LOCK-ON EFFECT

The lock-on effect in gallium arsenide may be observed by comparing the photocurrent decay times at low and high electric fields (see figure 4-2-1). The lock-on characteristic is that of persistent photocurrents with decay times that are extremely long compared to those at lower electric fields. This effect will limit the use of constant illumination switches to purely closing applications because the opening effect is destroyed by the onset of the persistent photocurrents. The name "lock-on" was given to describe how the loss of the opening effect was accompanied by a constant voltage mode of operation across the switch [2]. This constant voltage operating point is similar to that of a Zener diode. Typical lock-on voltages between 2.5 kV and 8.5 kV have been reported [2,11,19,38]. The reason lock-on is observed over a range of voltages for different samples is believed to be due to the various doping profiles and growth techniques.

The earliest explanations for the appearance of the lock-on effect were centered around the Gunn, or transferred electron, effect [24,27,28] based on the saturation of the electron drift velocity [2]. At low electric fields, the electron drift velocity varies linearly with the applied electric field. As the field is increased (typically to a few kilo-volts per centimeter), the electron drift velocity reaches a

maximum, experiences a negative slope, and then decays to a constant value. Gunn domains (high local electric fields) develop as electrons are moved to a higher quantum state, and begin to move at different velocities depending on their position in the material, which increases the magnitude of the high field region as the charges accumulate. These high field domains have been thought to have magnitudes high enough to cause impact ionization and carrier multiplication (this typically occurs at fields exceeding 200 kV/cm in GaAs).

A more recent description for the lock-on effect involves trap filling and double injection. Therefore the lock-on effect can also be described in terms of dark current as well as photocurrent behavior, neglecting impact ionization (for electric fields below a few hundred kV/cm). Instabilities in the dark I-V curves provide a mechanism to establish lock-on behavior without a source such as a laser or electron beam. A theoretical model has shown that the filling of deep traps causes a current controlled negative differential conductivity, and that the occupation numbers of the filled traps are spatially uniform across the sample during lock-on [49]. Once the filled trap scenario is established, the flux of holes entering from the cathode and the electrons from the anode no longer become depleted through trapping processes, and therefore they contribute to the drift current. The local space charge densities are reduced as a result of the trapping kinetics, and the current-voltage characteristics must change to a lower resistance state.